

Estimating long-term behavior of periodically driven flows without trajectory integration

Gary Froyland* Péter Koltai†

Abstract

Periodically driven flows are fundamental models of chaotic behavior and the study of their transport properties is an active area of research. A well-known analytic construction is the augmentation of phase space with an additional time dimension; in this augmented space, the flow becomes autonomous or time-independent. We prove several results concerning the connections between the original time-periodic representation and the time-extended representation, focusing on transport properties. In the deterministic setting, these include single-period outflows and time-asymptotic escape rates from time-parameterized families of sets. We also consider stochastic differential equations with time-periodic advection term. In this stochastic setting one has a time-periodic *generator* (the differential operator given by the right-hand-side of the corresponding time-periodic Fokker-Planck equation). We define in a natural way an autonomous generator corresponding to the flow on time-extended phase space. We prove relationships between these two generator representations and use these to quantify decay rates of observables and to determine time-periodic families of sets with slow escape rate. Finally, we use the generator on the time-extended phase space to create efficient numerical schemes to implement the various theoretical constructions. These ideas build on the work of [FJK13], and no expensive time integration is required. We introduce an efficient new hybrid approach, which treats the space and time dimensions separately.

1 Introduction

Periodically driven flows are fundamental testing grounds for many questions in nonlinear dynamics. Part of their attraction is their ability to create complicated dynamics even in two-dimensional phase space, and their suitability as models of many phenomena with periodic driving, due to biological, environmental, geophysical, or engineered cycles. The

*School of Mathematics and Statistics, University of New South Wales, Sydney NSW 2052, Australia. E-mail: g.froyland@unsw.edu.au

†Institute of Mathematics, Freie Universität Berlin, 14195 Berlin, Germany. E-mail: peter.koltai@fu-berlin.de

quantification of transport in dynamical systems has been intensely studied over recent decades [MMP84, RKLW90, Wig92, HP98, Are02, JW02, Wig05, SLM05, FP09, FPG14], from both geometric and probabilistic points of views. For certain periodically driven area-preserving flows [RKLW90] and two-dimensional maps [RKW90], the theory of lobe dynamics has helped explain how unions of pieces of stable and unstable manifolds of low period hyperbolic periodic points delineate “lobes” of fluid which are transported in a way organised by the manifolds. Our contributions in the present paper also concern the quantification of transport and span both geometric and probabilistic ideas.

We consider time-periodic flows on a compact state space $X \subset \mathbb{R}^d$ of the form

$$\dot{x}(t) = v(t, x(t)), \tag{1}$$

where $v : \tau S^1 \times X \rightarrow \mathbb{R}^d$ is a continuous vector field, and S^1 denotes the circle of unit circumference. One can rewrite (1) as an autonomous flow at the expense of adding an extra (time) dimension:

$$\dot{\theta}(t) = 1, \tag{2}$$

$$\dot{x}(t) = v(\theta(t), x(t)). \tag{3}$$

The central thread running through this paper is formalizing the connections between these two representations for various transport-related questions and exploiting these connections to compute several transport-related quantities, both theoretically and numerically.

First, we consider a fundamental transport question, namely, the computation of time-integrated flux through the boundaries of a time-periodic family of sets $A_t \subset X$, $t \in \tau S^1$. We show that this problem has a natural description in the time-extended domain and can be computed as an *instantaneous* flux through the time-extended set $\cup_{t \in \tau S^1} \{t\} \times A_t$ (Theorem 2). Our construction has a natural extension to the case of aperiodic velocity fields and aperiodic families of sets A_t .

Second, we turn to the time-asymptotic transport question of defining the rate of escape from a periodic collection of sets $\{A_t\}_{t \in \tau S^1}$. One can view this as considering an open dynamical system in a time-periodic flow, with an open domain $A_t \subset X$ that can itself be time-periodic. Trajectories vanish once they leave a set A_t at a time $t + k\tau$, $k \in \mathbb{Z}^+$. In discrete-time autonomous dynamical systems, $\Phi : X \rightarrow X$, one studies *escape rates* from a fixed set $A \subset X$: $E(A) = \limsup_{n \rightarrow \infty} (1/n) \log m(\bigcap_{i=0}^{n-1} \Phi^{-i} A)$, where m is normalised Lebesgue measure on X . The escape rate $E(A)$ measures the exponential rate of decay of the measure of the set of points x which “survive” for n steps ($x \in A, \Phi x \in A, \dots, \Phi^{n-1} x \in A$). We refer the reader to the excellent survey [DY06] for further background on escape rates in a discrete-time autonomous setting. Here, we generalise these ideas in two ways: firstly to continuous time, and secondly to periodic time-dependence. Under mild assumptions on the measurable and topological properties of this collection, we show that (i) the escape rate is not a time-dependent quantity (Theorem 10) and (ii) the escape rate in the original phase space X is identical to the escape rate of the autonomous flow in time-extended space (Theorem 11).

The notion of escape rates can be generalized to stochastic differential equations (SDEs) of the form

$$dx_t = v(t, x_t)dt + \varepsilon dw_t, \quad (4)$$

where $v : [0, \infty) \times X \rightarrow \mathbb{R}^d$ is a continuously differentiable, time-dependent vector field, $\{w_t\}_{t \geq 0}$ is a standard Wiener process, and $\varepsilon \geq 0$ is a parameter describing the standard deviation of the Wiener process. We define a probabilistic description of escape rate and in Proposition 14 we show that, for periodically driven SDEs, the escape rate computed in the original phase space X has the same value as the escape rate of the associated autonomous SDE in time-extended space.

Connections between the Perron–Frobenius operator and escape rates for time-homogeneous diffusion processes have been considered in [SHM03, HMS04]. In the discrete-time deterministic setting, it was established in [FS10] that eigenfunctions of the Perron–Frobenius operator $\mathcal{P} : L^1(X, m) \circlearrowleft$ corresponding to eigenvalues close to 1, so-called *strange eigenmodes*, can be used to create subsets $A \subset X$ with slow escape rate. More precisely, if $\mathcal{P}f = \lambda f$, $0 < \lambda < 1$, then the sets $A^+ = \{f \geq 0\}$, $A^- = \{f < 0\}$ both have escape rates slower than $\log \lambda$. These statements are generalized in [FS13] to random discrete-time systems and in [FJK13] to discrete-time systems with i.i.d. noise. In Theorem 16 we first extend this result to the continuous time setting for SDEs of the form:

$$dx_t = v(x_t)dt + \varepsilon dw_t. \quad (5)$$

In Theorem 19 we then further generalize the result to general non-homogeneous SDEs of the form (4), where $v : [0, \infty) \times X \rightarrow \mathbb{R}^d$ need not be periodic in t . In this latter generalization, one chooses an essentially bounded function $f : X \rightarrow \mathbb{R}$ so that

$$\limsup_{t \rightarrow \infty} \frac{1}{t} \log \|\mathcal{P}_{s,t}f\|_{L^1} = \lambda < 0.$$

Here, $\mathcal{P}_{s,t}$ denotes the Perron–Frobenius operator (also called the transfer operator) that pushes forward densities from time s to time $t \geq s$. Under mild topological assumptions on the time-dependent family of sets $A_t := \{\mathcal{P}_{s,t}f \geq 0\} \subset X$, we show that the escape from this family is slower than the Lyapunov exponent (or decay rate) λ . Returning to the periodic driving setting, where $v(t, \cdot) = v(t + k\tau, \cdot)$, $k \in \mathbb{Z}^+$, we demonstrate that the family of functions that produce the slowest decay rate are the periodic family $\{f_s\}_{s \in \tau S^1}$ corresponding to the second largest eigenvalue of $\mathcal{P}_{s,s+\tau}$ (Proposition 20).

In the final theoretical section, we consider time-extended SDEs of the form:

$$d\theta_t = dt, \quad (6)$$

$$dx_t = v(\theta_t, x_t)dt + \varepsilon dw_t, \quad (7)$$

where $v : \tau S^1 \times X \rightarrow \mathbb{R}^d$. We construct a time-extended generator \mathcal{G} for this time-extended SDE and identify the time fibres of eigenfunctions of \mathcal{G} as equivariant functions under $\mathcal{P}_{s,s+t}$ (Lemma 22). Theorem 23 then states that the slowest decaying family of functions $\{f_t\}_{t \in \tau S^1}$ can be obtained as time fibres of the eigenfunction \mathbf{f} corresponding to the eigenvalue of \mathcal{G}

with second largest real part. We discuss how to interpret complex eigenvalues and eigenfunctions of \mathcal{G} (they describe periodic motions different to the driving period), and other properties of the point spectrum of \mathcal{G} , including how numerical methods distort the spectrum. To give the reader an overview, we partially summarize our findings graphically in Figure 3.

In the numerical section we describe in detail two numerical methods for approximating \mathcal{G} . First, an extension of the Ulam Galerkin approach from [FJK13], and second, a new, efficient hybrid approach, which uses Fourier collocation in the time direction to take advantage of the special dynamics in that coordinate. We apply the full Ulam numerics to analyse an SDE version of the periodically driven double gyre flow [FPG14], finding that the largest transport barrier is a smoothed analogue of the unstable manifold of a hyperbolic periodic point on the boundary of the domain. Boundaries of well-known regions of elliptic dynamics are determined as the sets with the next smallest escape rate. We numerically check Theorem 19 by explicitly computing escape rates using simulated trajectories and verify that the escape rates are indeed slower than indicated by the corresponding eigenvalue of \mathcal{G} . Similar computations are performed for the Bickley jet [RBBV⁺07] using the hybrid approach to approximating \mathcal{G} . We determine transport barriers and vortices in regions similar to previous work [RBBV⁺07, FSM10, BVOB⁺10, HBV12], but we can do this *without any expensive trajectory integration* and additionally obtain numerical estimates of transport rates such as escape rates and decay rates. Furthermore, by utilizing information carried in complex eigenvalues, we are able to detect previously unknown slowly decaying structures with *periods different to the driving period*; building upon similar observations [SSA09, FGTQ14] for discrete-time autonomous dynamics.

2 Accumulated outflow from a time-periodic family of sets

Suppose we have a compact state space $X \subset \mathbb{R}^d$ and a time-dependent, continuous vector field $v : \mathbb{R} \times X \rightarrow \mathbb{R}^d$. We assume that the time-dependence is periodic with period τ , i.e. $v : \tau S^1 \times X \rightarrow \mathbb{R}^d$. Let a family $\{A_t\}_{t \in \tau S^1}$ of subsets of X be given, such that

Assumption 1:

- (a) for every $t \in \tau S^1$, the boundary ∂A_t of A_t is parametrized by the piecewise smooth function $a(t, \cdot) : R \rightarrow \mathbb{R}^d$ over some parameter domain $R \subset \mathbb{R}^{d-1}$; and
- (b) for every $t \in \tau S^1$ and $x \in \partial A_t$, there is a unique $r \in R$ with $a(t, r) = x$, and the function $w(t, x) = \frac{\partial}{\partial t} a(t, r)$ is well-defined. We think of $w(t, x)$ as the instantaneous velocity of the boundary of A_t at $x \in A_t$.

The *cumulative outflow flux* from the family of sets over a period of the vector field is then given by

$$\int_{\tau S^1} \int_{\partial A_t} \langle v(t, x) - w(t, x), n_t(x) \rangle^+ d\sigma(x) dt, \quad (8)$$

where $\langle \cdot, \cdot \rangle$ denotes the Euclidean inner product, $n_t(x)$ denotes the unit outer normal on ∂A_t at x , the superscript $+$ denotes the positive part, i.e. $f^+ := \max\{0, f\}$, and $d\sigma(\cdot)$ denotes integration with respect to co-dimension 1 volume on X . It can clearly be seen that the cumulative outflow is zero if the velocities of the boundaries of the family of sets A_t match the vector field v , i.e. if $v \equiv w$.

Let us now consider the *augmented* state space $\mathbf{X} = \tau S^1 \times X$ with elements $(\theta, x) = \mathbf{x} \in \mathbf{X}$, and the augmented ODE

$$\dot{\theta}(t) = 1 \tag{9}$$

$$\dot{x}(t) = v(\theta(t), x(t)) \tag{10}$$

We define the augmented vector field $\mathbf{v} : \mathbf{X} \rightarrow \mathbb{R}^{d+1}$ by $\mathbf{v}(\theta, x) = (1, v(\theta, x))^T$, and denote its flow map by $\phi^t : \tau S^1 \times X \rightarrow \tau S^1 \times X$. Note that this dynamical system is autonomous in the extended phase space. Using the periodic family $\{A_\theta\}_{\theta \in \tau S^1}$ we define the *augmented set*

$$\mathbf{A} = \bigcup_{\theta=0}^{\tau} \{\theta\} \times A_\theta, \tag{11}$$

Considering the autonomous system defined by $\dot{\mathbf{x}} = \mathbf{v}(\mathbf{x})$ acting on the augmented state space, we can define the *instantaneous outflow flux* from the set \mathbf{A} by

$$\int_{\partial \mathbf{A}} \langle \mathbf{v}(\mathbf{x}), \mathbf{n}(\mathbf{x}) \rangle^+ d\sigma(\mathbf{x}), \tag{12}$$

where $\mathbf{n}(\mathbf{x})$ is the unit outer normal on $\partial \mathbf{A}$ at \mathbf{x} and $d\sigma(\cdot)$ denotes integration with respect to co-dimension 1 volume on \mathbf{X} . Note that conditions (a) and (b) from above imply that \mathbf{n} exists and is well-defined almost everywhere on $\partial \mathbf{A}$.

Theorem 2: For a continuous time-periodic vector field and a time-periodic family $\{A_\theta\}_{\theta \in \tau S^1}$ of sets satisfying the conditions of Assumption 1, the cumulative outflow flux and the instantaneous outflow flux in augmented space are equal:

$$\int_{\tau S^1} \int_{\partial A_\theta} \langle v(\theta, x) - w(\theta, x), n_\theta(x) \rangle^+ d\sigma(x) d\theta = \int_{\partial \mathbf{A}} \langle \mathbf{v}(\mathbf{x}), \mathbf{n}(\mathbf{x}) \rangle^+ d\sigma(\mathbf{x}). \tag{13}$$

Both sides of equation (13) are independent of the chosen parametrization a in Assumption 1.

Proof. See Appendix A.1. □

Remark 3: An analogous statement to that of Theorem 2 can be shown to also hold in the case when time and the family of sets is not periodic, but evolves in a finite interval, $t \in [t_0, t_1]$. Then, however, one has to integrate over the “spatial boundary” of the augmented set \mathbf{A} , i.e. $\bigcup_{t \in [t_0, t_1]} \{t\} \times \partial A_t$, the boundary in the x coordinate direction.

This computation is related to a recent calculation [Kar16] of Lagrangian flux through a surface, as opposed to Eulerian flux considered here.

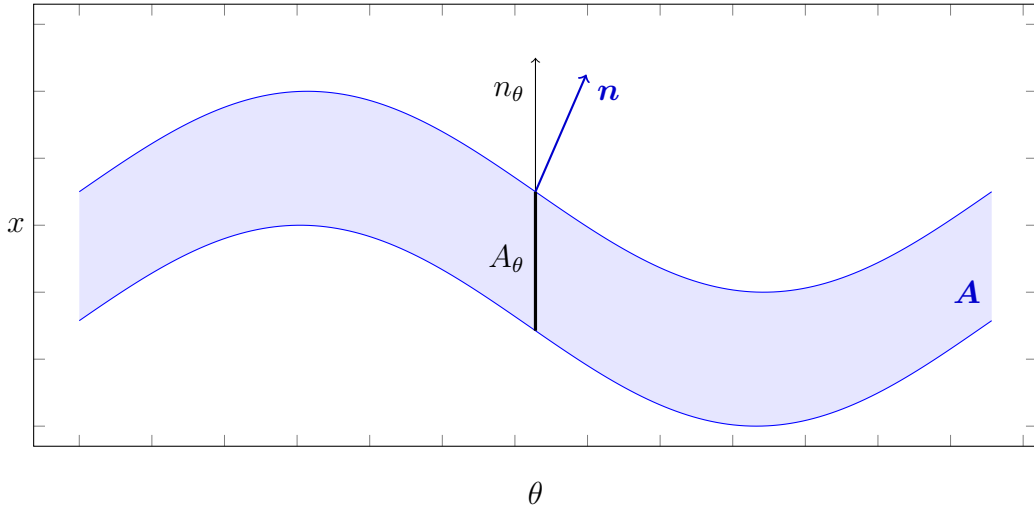


Figure 1: Graphical representation of some objects from Theorem 2. The thick black segment is one specific A_θ with a unit normal vector n_θ . The “trace” of all sets A_θ in \mathbf{X} is the augmented set \mathbf{A} , shown by the blue shaded region, and having unit outer normal \mathbf{n} .

3 Time-asymptotic escape rates from a time-periodic family of sets

The purpose of this section is to introduce a description of coherence for deterministic dynamics for long flow times that admits an immediate generalization to stochastically perturbed systems. We then state a result analogous to Theorem 2 for this alternative coherence descriptor.

3.1 The survivor set

Define ϕ_{t_1, t_2} to be the flow map of the ODE $\dot{x}(t) = v(t, x(t))$ from time t_1 to $t_2 \geq t_1$, with the convention $\phi_{t_1, t_2} = (\phi_{t_2, t_1})^{-1}$ if $t_2 < t_1$. This latter case refers to integration backward in time.

Let some family of Borel measurable sets $\{A_\theta\}_{\theta \in \tau S^1}$ be given. For practical reasons, we will assume that the family of sets $\{A_\theta\}$ is “nice”.

Definition 4: A family of measurable sets $\{A_\theta\}_{\theta \in \tau S^1}$ is called *nice*, if

- (a) A_θ is closed and has nonempty interior for every $\theta \in \tau S^1$.
- (b) The temporal evolution of the A_θ is continuous, i.e. $h(A_\theta, A_{\theta+\sigma}) \rightarrow 0$ as $\sigma \rightarrow 0$ for all $\theta \in \tau S^1$. Here $h(\cdot, \cdot)$ refers to the Hausdorff-distance of two sets.

While in the previous section we have been looking at what *leaves* a family of sets, here we will focus on what *stays* inside, as measured by Lebesgue measure m . For this,

we will allow arbitrary large times (thinking of the system running over many periods), hence we identify τS^1 with $[0, \tau)$ and for any $t \in \mathbb{R}$ we identify A_t with $A_{t \bmod \tau}$. Let $A_{s,t} := \bigcap_{r=s}^t \phi_{r,s} A_r = \{x \in X \mid \phi_{s,r} x \in A_r \forall r \in [s, t]\}$ denote the t -survivor set at anchor time s , i.e. the set of points at time s that stay in the family $\{A_r\}$ until time t . We will refer to it simply as “survivor set” if anchor time and duration are clear. Note that the intersection is taken over pre-images of sets under the flow.

Proposition 5: Let $\{A_t\}$ be a nice family of sets. Then

1. $A_{s,t}$ is measurable; and
2. for any sequence $(r_i)_{i \in \mathbb{N}} \subset \mathbb{R}$ which is dense¹ in the interval (s, t) one has $\lim_{n \rightarrow \infty} m(\bigcap_{i=1}^n \phi_{r_i, s} A_{r_i}) = m(A_{s,t})$.

Proof. See Appendix A.2. □

For *volume-preserving* flows there is a simple relation between the measure of the survivor set and the outflow flux. Since the proof of this is cumbersome and does not further contribute to the exposition, we only give the main idea, and motivate this idea by an example. Note that a family of closed sets with non-empty interior satisfying Assumption 1 of the previous section is also nice.

Proposition 6: Let $\{A_\theta\}$ be a family of closed sets with non-empty interior satisfying Assumption 1. Further, let $v(t, \cdot)$ be divergence-free for all times t . Then, the volume of the surviving set is monotonically decreasing in t for fixed s and satisfies at its points of differentiability

$$0 \geq \frac{d}{dt} m(A_{s,t}) \geq - \int_{\partial A_t} \langle v(t, x) - w(t, x), n_t(x) \rangle^+ d\sigma(x). \quad (14)$$

Idea of the proof. Proposition 6 essentially states that the rate at which the survivor set loses measure is at most the outflow flux. To see this, note that $A_{s,t}$ will decrease in measure if $\phi_{s,r} A_{s,t} \not\subseteq A_r$ for some $r > t > s$. Considering times only infinitesimally greater than t , this means that $\phi_{s,t} A_{s,t}$ and A_t have to share a part of their boundary where the integrand in (14) is positive, for $m(A_{s,t})$ to decrease. Since the right-hand side of (14) does not take this into account (it integrates over the whole boundary of A_t not just over the common part with $\phi_{s,t} A_{s,t}$), it overestimates the decay of the volume of the survivor set. The second inequality in (14) becomes an equality if every $x \in \partial A_t$ where $\langle v(t, x) - w(t, x), n_t(x) \rangle \geq 0$ is also a boundary point of $\phi_{s,t} A_{s,t}$. □

Example 7: Let $X = S^1$, $v(t, x) = 0.3 \cos(t)$, and $A_t = [0.3 + 0.2 \sin(t), 0.7 + 0.2 \sin(t)] \subset X$. Then, for $t \in [0, \pi/2]$ trajectories leave A_t at the upper boundary, and $A_{0,t} = [0.3, 0.7 - 0.1 \sin(t)]$. For $t \in [\pi/2, \pi]$, there is no loss in the measure of the survivor set $A_{0,t}$, because $\phi_{0,t} A_{0, \pi/2} \subset A_t$. For $t > \pi$, trajectories which initially started in A_0 may leave A_t on its lower boundary. The survivor sets and their images are shown in Figure 2. Note that

¹A sequence $(r_i) \subset S$ is called dense in a set S , if for any $s \in S$ there is a subsequence $r_{i_j} \rightarrow s$ as $i_j \rightarrow \infty$.

for $\pi/2 < t < \pi$ no trajectory that initially started in A_0 leaves $\{A_r\}$, because for these times the blue and grey regions do not share a common boundary. Nevertheless, the integral in (14) is positive, hence overestimates the decay of the survivor set, showing a strict inequality.

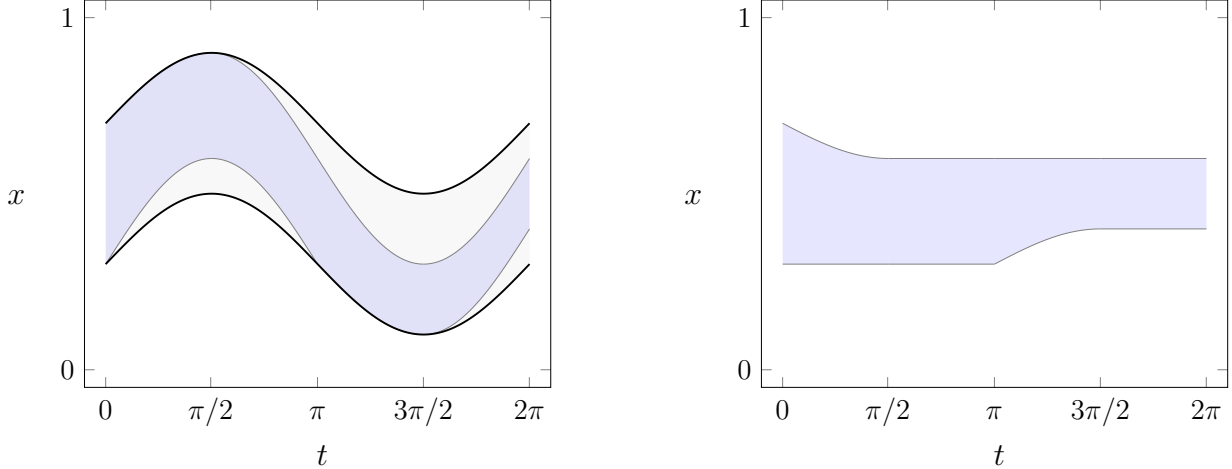


Figure 2: Graphical representation of Example 7. Left: the thick black lines enclose the sets A_t (light gray shaded region), and the blue shaded region in it is the image of the survivor set $A_{0,t}$, i.e. $\phi_{0,t}A_{0,t}$, for times 0 to 2π . Right: the shaded region shows the survivor set $A_{0,t}$ versus t .

3.2 Escape rates

Since we think of the system running for large times (many periods), we are going to look at time-asymptotic quantities, as $t \rightarrow \infty$.

Recall Proposition 5, stating that the survivor set is measurable. Thus, we can make the following definition for escape rate in continuous time.

Definition 8: The (lower) escape rate for a nice family of sets $\{A_r\}_{r \geq s}$, starting at some time s , is given by

$$E(\{A_r\}_{r \geq s}) = - \limsup_{t \rightarrow \infty} \frac{1}{t-s} \log m \left(\bigcap_{r=s}^t \phi_{r,s} A_r \right) = - \limsup_{t \rightarrow \infty} \frac{1}{t-s} \log m (A_{s,t}). \quad (15)$$

Using the augmented flow ϕ and augmented set \mathbf{A} defined by (11), we may also consider the escape rate from this set, given by

$$\mathbf{E}(\mathbf{A}) = - \limsup_{t \rightarrow \infty} \frac{1}{t} \log m \left(\bigcap_{r=0}^t \phi_{-r} \mathbf{A} \right), \quad (16)$$

where m denotes the Lebesgue measure on \mathbf{X} . Our goal is to show that (15)=(16). Before stating a theorem in this direction, we interpret $\bigcap_{r=0}^t \phi_{-r} \mathbf{A}$ in terms of the time-fibred

representation:

$$\begin{aligned}
\bigcap_{r=0}^t \phi_{-r} \mathbf{A} &= \bigcap_{r=0}^t \phi_{-r} \left(\bigcup_{\theta=0}^{\tau} \{\theta\} \times A_{\theta} \right) &= \bigcap_{r=0}^t \bigcup_{\theta=0}^{\tau} (\{\theta - r\} \times \phi_{\theta, \theta-r} A_{\theta}) \\
&= \bigcup_{\theta'=0}^{\tau} \{\theta'\} \times \bigcap_{\substack{r=0 \\ \theta=\theta'+r}}^t \phi_{\theta, \theta-r} A_{\theta} \\
&\stackrel{r'=\theta'+r}{=} \bigcup_{\theta'=0}^{\tau} \{\theta'\} \times \bigcap_{r'=\theta'}^{t+\theta'} \phi_{r', \theta'} A_{r'} \\
&= \bigcup_{\theta'=0}^{\tau} \{\theta'\} \times A_{\theta', \theta'+t}, \tag{17}
\end{aligned}$$

where the second line is obtained by noting that intersections of the augmented sets are non-empty only if $\theta - r = \theta' = \text{const}$. Thus, the set $\bigcap_{r=0}^t \phi_{-r} \mathbf{A}$ in augmented space is the natural augmentation (via a time-union) of the fibre-wise survivor sets $A_{\theta', \theta'+t}$.

Remark 9: It is natural to ask whether the continuous time escape rates we consider here are also connected to escape rates for the Poincaré return map of the dynamics. The latter would be defined by a discrete-time version of (15), namely:

$$-\limsup_{n \rightarrow \infty} \frac{1}{n\tau} \log m \left(\bigcap_{k=0}^{n-1} \phi_{s+k\tau, s} A_{s+k\tau} \right). \tag{18}$$

Clearly, because the set formed by the discrete intersection in (18) contains the set formed by the continuous intersection in (15), the escape rate for the Poincaré return map will be slower than for the continuous flow. See also [FJK13, section 3.3] for a discussion of escape rates of flow maps in both the deterministic and stochastic cases.

Our first result regarding escape rates is that $E(\{A_r\}_{r \geq s})$ is independent of s .

Theorem 10: For every $s_1, s_2 \in \tau S^1$ one has

$$E(\{A_r\}_{r \geq s_1}) = E(\{A_r\}_{r \geq s_2}).$$

Proof. See Appendix A.3. □

To express the independence of the starting time we write from now on $E(\{A_r\})$ for the escape rate from the family $\{A_r\}$ of sets. Our second result on escape rates is that the two definitions (15) and (16) are equivalent.

Theorem 11: If $\{A_r\} \subset X$ is a nice family of sets and $v : \tau S^1 \times X \rightarrow \mathbb{R}^d$ is a continuous, time-periodic vector field, then

$$E(\{A_r\}) = \mathbf{E}(\mathbf{A}),$$

Proof. See Appendix A.4. □

4 Time-asymptotic escape rates for SDEs from a time-periodic family of sets

Many processes in nature are modeled through dynamics perturbed by random noise and we wish to extend our results to this case as well. Unfortunately, the mathematical framework presented in Theorem 2 is not suitable for handling this situation, because the outflow flux induced by the stochastic forcing is infinite. To see this, note that the mean displacement of a standard Brownian motion in a time interval of length dt is \sqrt{dt} . The volume of the portion of state space that can leave A_t in this time interval is thus potentially of order \sqrt{dt} , giving an instantaneous flux of order $(dt)^{-1/2}$, which diverges as $dt \rightarrow 0$. On the other hand, escape rates can easily be generalized to cope with the stochastic situation.

To facilitate presentation, we assume from now on that the vector field at hand is divergence-free, thus the (deterministic) flow $\phi_{s,t}$ preserves the Lebesgue measure, meaning that $m \circ \phi_{t,s} = m$ for every $t \geq s$. We will need the following regularity assumptions:

Assumption 12:

- (a) The state space X is a bounded domain in \mathbb{R}^d , uniformly regular of class C^4 . In particular, its boundary is a C^4 -manifold.
- (b) The vector field is continuously differentiable on the closure of X for all times, i.e. $v(\theta, \cdot) \in C^1(\bar{X}, \mathbb{R}^d)$, and it is continuously differentiable in time, i.e. the mapping $\theta \mapsto v(\theta, x)$ is in $C^1(\tau S^1, \mathbb{R}^d)$ for every $x \in \bar{X}$. Further, v is tangential to ∂X on the boundary ∂X for all times.

From now on we will consider small random perturbations of the deterministic dynamics. These are stochastic processes $\{x_t\}_{t \geq s}$ governed by the Itô differential equation

$$dx_t = v(t, x_t)dt + \varepsilon dw_t, \tag{19}$$

where $\{w_t\}_{t \geq s}$ is a d -dimensional standard Wiener process [Øks03], and $\varepsilon > 0$ is a parameter which is assumed to be small compared with the magnitude of the vector field.² Also, we take reflecting boundary conditions, i.e. no realizations of the process $\{x_t\}$ are allowed to leave X at any times.

Escape rates for SDEs [HMS04] are defined through the probability distribution of the process:

Definition 13: The (*lower*) *escape rate* for a nice family of sets $\{A_r\}_{r \geq s}$, starting at some

²For simplicity, we are only considering noise with constant coefficients. Nevertheless, all the following statements hold true if ε is replaced by $\sigma(t, x)$, such that $\sigma \in C^1(\tau S^1 \times \bar{X}, \mathbb{R}^{d \times d})$, and $\sigma(\theta, x)$ is uniformly positive definite in θ and x .

time s , is given by

$$\begin{aligned} E(\{A_r\}_{r \geq s}) &= -\limsup_{t \rightarrow \infty} \frac{1}{t-s} \log \mathbb{P}_{x_s \sim m} (x_r \in A_r \ \forall r \in [s, t]) \\ &= -\limsup_{t \rightarrow \infty} \frac{1}{t-s} \log \mathbb{P}_{x_s \sim m} \left(\bigcap_{r \in [s, t]} \{\omega \mid x_r(\omega) \in A_r\} \right). \end{aligned}$$

where m denotes the Lebesgue measure, $x_s \sim m$ means that the random variable x_s has distribution m , and ω represents a realization of the noise process from a probability space which we do not specify here further.

The existence of $E(\{A_r\})$ requires the \mathbb{P} -measurability of the event

$$\bigcap_{r \in [s, t]} \{\omega \mid x_r(\omega) \in A_r\}.$$

One can follow the proof of Proposition 5, using the continuity of sample paths³ to obtain the measurability of $\mathcal{E} := \bigcap_{r \in [s, t]} \{\omega \mid x_r(\omega) \in A_r\}$ for a family $\{A_r\}$ of nice sets.

If the vector field is time-independent, the process $\{x_r\}$ is (*time-*)*homogeneous* (i.e. $\mathbb{P}_{x_s=y}(x_t \in A) = \mathbb{P}_{x_{s+r}=y}(x_{t+r} \in A)$ for every $r \geq 0$, $s \leq t$, and $A \in \mathfrak{B}$). Here, and in the following, \mathfrak{B} denotes the Borel sigma algebra on X . Then, the escape rate from a single closed set $A \in \mathfrak{B}$ is well defined,

$$\begin{aligned} E(A) &= -\limsup_{s \rightarrow \infty} \frac{1}{t-s} \log \mathbb{P}_{x_s \sim m} (x_r \in A \ \forall r \in [s, t]) \\ &= -\limsup_{s \rightarrow \infty} \frac{1}{t-s} \log \mathbb{P}_{x_s \sim m} \left(\bigcap_{r \in [s, t]} \{\omega \mid x_r(\omega) \in A\} \right). \end{aligned}$$

Before we go on to find families of sets with low escape rates, we generalize the result of Theorem 11 to the noisy dynamical setting. To this end, note that the non-homogeneous SDE $dx_t = v(t, x_t)dt + \varepsilon dw_t$ can be made homogeneous by augmenting the state space, exactly as before:

$$\begin{aligned} d\theta_t &= dt, \\ dx_t &= v(\theta_t, x_t)dt + \varepsilon dw_t, \end{aligned} \tag{20}$$

or, alternatively,

$$d\mathbf{x}_t = \mathbf{v}(\mathbf{x}_t)dt + \boldsymbol{\varepsilon} d\mathbf{w}_t \tag{21}$$

where the augmented state \mathbf{x} and vector field \mathbf{v} are as before, $\{\mathbf{w}_t\}$ is a $(d+1)$ -dimensional standard Wiener process, and

$$\boldsymbol{\varepsilon} = \begin{pmatrix} 0 & 0 \\ 0 & \varepsilon I_{d \times d} \end{pmatrix} \in \mathbb{R}^{(d+1) \times (d+1)},$$

with $I_{d \times d} \in \mathbb{R}^{d \times d}$ being the identity matrix.

³i.e. that $t \mapsto x_t$ is a continuous function for \mathbb{P} -a.e. ω ; cf. [Oks03].

Proposition 14: Let $\{A_r\}_{r \in \tau S^1}$ be a family of sets and $\mathbf{A} \subset \tau S^1 \times X$ the associated augmented set, cf. (11). Let $E(\{A_r\})$ denote the escape rate of the process $\{x_r\}_{r \geq s}$ governed by (19) from the family $\{A_r\}$ of sets, as defined in Definition 13. Let $\mathbf{E}(\mathbf{A})$ denote the escape rate of the associated augmented process $\{\mathbf{x}_r\}$ governed by (21) from the augmented set \mathbf{A} . Then, we have

$$E(\{A_r\}) = \mathbf{E}(\mathbf{A}).$$

Proof. By (20) and (21) we can identify x_r with the last d coordinates of \mathbf{x}_r , and the time r with the first coordinate of \mathbf{x}_r . Thus, we can also identify the probability laws of these two processes (given $x_s \sim m$ and $\mathbf{x}_s \sim \delta_s \otimes m$). With

$$x_r \in A_r \iff \mathbf{x}_r \in \{r\} \times A_r \subset \mathbf{A}$$

the claim follows from the fact that for time-periodic forcing the escape rates are independent on starting time, and that the time-fibers of the Lebesgue measure \mathbf{m} on $\tau S^1 \times X$ is the Lebesgue measure m , independently of the fiber chosen (recall that we chose the initial distribution for escape rates to be Lebesgue). \square

Now we turn to the questions of (i) whether there are coherent families of sets with small escape rates, and (ii) how to find them.

5 Finding families with low escape rates

5.1 The transfer operator and its infinitesimal generator

The evolution of the system (19) is characterized by the time-parametrized family of *stochastic transition function* $p_{s,t} : X \times \mathfrak{B} \rightarrow [0, 1]$, $t \geq s$,

$$p_{s,t}(y, A) = \mathbb{P}_y(x_t \in A),$$

describing the probability distribution of the process, given it started in $x_s = y \in X$ a.s. (almost surely). The stochastic transition function $p_{s,t}(y, \cdot)$ can be shown to be absolutely continuous with respect to the Lebesgue measure for a.e. (almost every) $y \in X$ (cf. [LM94, Section 11.6]), and thus there is a family of *transition density functions* $\{q_{s,t}\}_{t \geq s}$, with

$$p_{s,t}(y, A) = \int_A q_{s,t}(y, z) dm(z) \quad \text{for a.e. } y \in X.$$

If the initial condition x_s is only given by its density function f , the probability distribution of x_t is

$$\mathbb{P}_{x_s \sim f}(x_t \in A) = \int_A \int_X q_{s,t}(y, z) f(y) dm(y) dm(z).$$

Note that the probability measure $\mathbb{P}_{x_s \sim f}(x_t \in \cdot)$ is absolutely continuous with respect to m : we denote its Radon–Nikodým derivative by f_t . The (linear) operator mapping f to f_t is called the *transfer operator* $\mathcal{P}_{s,t}$,⁴ and is given by

$$\mathcal{P}_{s,t}f := \int_X q_{s,t}(y, \cdot) f(y) dm(y).$$

We will see below that, due to v being divergence-free for all times, $\mathcal{P}_{s,t}\mathbb{1} = \mathbb{1}$ for every $s \leq t$, and thus $\mathcal{P}_{s,t} : L^r(X) \rightarrow L^r(X)$ is a well-defined contraction for every $1 \leq r \leq \infty$; cf. [BR95, Lemma 1]. The function $\mathbb{1}$ is the a.e. constant function on X with value 1.

Suppose that $f_t(x)$ and $v(t, x)$ are C^2 functions with respect to both t and x . Then, $g(t, \cdot) = f_t$ solves the *Fokker–Planck* equation [LM94, Section 11.6]

$$\partial_t g(t, x) = \frac{\varepsilon^2}{2} \Delta g(t, x) - \operatorname{div}(g(t, \cdot) v(t, \cdot))(x), \quad g(0, x) = f(x), \quad \left. \frac{\partial g(t, \cdot)}{\partial n} \right|_{\partial X} = 0, \quad (22)$$

where $\Delta = \sum_{i=1}^d \partial_{x_i}^2$ denotes the Laplace operator, and $\operatorname{div} = \sum_{i=1}^d \partial_{x_i}$ denotes the divergence operator on X , and $\frac{\partial}{\partial n}$ is the normal derivative on the boundary.

Assume for a moment that $v(t, x) = v(x)$, i.e. the vector field doesn't depend on time. Then, $\mathcal{P}_{s,t}$ only depends on $t - s$, and for simplicity we write \mathcal{P}_t . The *semigroup property* holds: $\mathcal{P}_{t+s} = \mathcal{P}_t \mathcal{P}_s$ for every $s, t \geq 0$. We define the operator

$$\mathcal{G}f = \lim_{t \rightarrow 0} \frac{\mathcal{P}_t f - f}{t} \quad (\text{convergence in } L^r). \quad (23)$$

$\mathcal{G} : D(\mathcal{G}) \rightarrow L^r(X)$ is called the (*infinitesimal*) *generator* of the semigroup of operators $\{\mathcal{P}_t\}_{t \geq 0}$, and $D(\mathcal{G})$ is its domain, i.e. the set containing all $f \in L^r(X)$ where the limit (23) exists. If $f \in C^2(X, \mathbb{R})$, then $f \in D(\mathcal{G})$, and $\mathcal{G}f = \frac{1}{2}\varepsilon^2 \Delta f - \operatorname{div}(fv)$, hence \mathcal{G} is the operator building the right hand side of the Fokker–Planck equation (22). That \mathcal{G} indeed “generates” $\{\mathcal{P}_t\}$ is underlined by the following result.

Proposition 15 (Spectral Mapping Theorem [Paz83, Theorem 2.2.4]): For $f \in L^r(X)$ and $\lambda \in \mathbb{C}$ one has $\mathcal{G}f = \lambda f$ iff $\mathcal{P}_t f = \exp(\lambda t)f$ for every $t \geq 0$.

Essentially, all the information contained in the family $\{\mathcal{P}_t\}$ is also contained in a single operator, \mathcal{G} . To work directly with the generator has some advantages, if one is to (numerically) compute quantities of interest related to dynamical systems. This has been exploited e.g. in [FJK13]. In the non-autonomous setting a general result such as Proposition 15 does not exist, however if f_t is sufficiently smooth, it satisfies $\partial_t f_t = \mathcal{G}_t f_t$, where \mathcal{G}_t is the infinitesimal generator associated with the vector field $v_t := v(t, \cdot)$, i.e. $\mathcal{G}_t f = \frac{1}{2}\varepsilon^2 \Delta f - \operatorname{div}(f v_t)$. This also shows that if $v(t, \cdot)$ is divergence-free for all t , then $\mathcal{G}_t \mathbb{1} = 0$ for all t , and hence $\mathcal{P}_{s,t} \mathbb{1} = \mathbb{1}$ for all $s \leq t$.

⁴In the field of operator semigroups (see below, or, for instance [EN00]) the family of transfer operators, $\{\mathcal{P}_{s,t}\}_{t \geq s}$, is also called *evolution family*.

5.2 Lyapunov exponents and escape rates

Escape rates for homogeneous processes. The following theorem extends results obtained in [FS10, FS13, FJK13], to continuous time stochastic processes. It states that for eigenfunctions of \mathcal{G} with decay rate λ , the positive and negative supports of the function determine sets from which the escape rate is slower than the decay rate λ .

Theorem 16: For a homogeneous stochastic process $\{x_t\}_{t \geq 0}$ with almost surely continuous sample paths (cf. [Øks03]), let $\{\mathcal{P}_t\}_{t \geq 0}$ denote the associated transfer operator semigroup on $L^1 = L^1_m$. Let $f \in L^1 \cap L^\infty$ be such that $\mathcal{P}_t f = e^{\lambda t} f$ for a $\lambda < 0$. Let us further assume that $A^\pm := \{\pm f \geq 0\}$ is closed. Then $E(A^\pm) \leq -\lambda$.

Proof. See Appendix A.5. □

The case $\lambda \notin \mathbb{R}$ has been considered in [FJK13] and in Remark 24 below we extend these results as well to the non-autonomous (non-homogeneous) setting.

Escape rates for non-homogeneous processes. If we are looking for a non-homogeneous version of Theorem 16, it is to be expected that the role of *one* function f is going to be taken by a whole *family* of functions $\{f_r\}$. To assume that the temporal change in sets like $\{f_t \geq 0\}$ is everywhere continuous might be too optimistic. We thus weaken the notion of niceness introduced in Definition 4:

Definition 17 (Sufficiently nice family of sets): A *sufficiently nice* family of sets $\{A_r\}_{r \in \mathcal{I}}$, for an interval $\mathcal{I} \subset \mathbb{R}$, is such that

- (i) for every $r \in \mathcal{I}$ the set A_r is closed; and
- (ii) the function $\sigma \mapsto h(A_r, A_{r+\sigma})$ is either left- or right-continuous at $\sigma = 0$ for every $r \in \mathcal{I}$.

We also introduce *decay rates* as a function-based version of the set-based escape rates.

Definition 18 (Lyapunov exponents): Given a $f \in L^1_m$, the *Lyapunov exponent* of f with respect to initial time s is defined as the decay rate of the norm of f while transported by the transfer operator:

$$\Lambda_s(f) := \limsup_{t \rightarrow \infty} \frac{1}{t-s} \log \|\mathcal{P}_{s,t} f\|_1. \quad (24)$$

We have the following:

Theorem 19: Given $f \in L^1 \cap L^\infty$, $\int f = 0$, define the family of sets $\{A_r^\pm\}_{r \geq s}$ by $A_r^\pm = \{\pm \mathcal{P}_{s,r} f \geq 0\}$. Suppose that $\{A_r^\pm\}$ is a sufficiently nice family. Then $E(\{A_r^\pm\}) \leq -\Lambda_s(f)$.

Proof. See Appendix A.6. □

Theorem 19 states that if we find a function with a low decay rate Λ (a “low” decay means Λ is small negative, i.e. close to zero), than we readily have a pair of sets with coherence (escape) rate at least as low as the decay rate Λ . Thus, we aim for finding functions with low decay rates. Note that since $\mathcal{P}_{s,t} \mathbb{1} = \mathbb{1}$ for all $s \leq t$, any function not perpendicular to $\mathbb{1}$, i.e. satisfying $\int f \neq 0$, will have a decay rate $\Lambda = 0$, because $\|\mathcal{P}_{s,t} f\|_1 \not\rightarrow 0$ as $t \rightarrow \infty$.

In general, properties of interest in periodically forced nonlinear dynamical systems can be characterized by those of the associated *Poincaré return map*, the map describing the time- τ -evolution of the system with forcing period τ . By considering the transfer operator for a single period τ we have the following simple characterization of the slowest decaying family of functions.

Proposition 20: For every $s, \tilde{s} \in \tau S^1$ we have

$$\max_{f \neq 0} \Lambda_s(f) = \frac{1}{\tau} \log |\lambda_2(\mathcal{P}_{s,s+\tau})| = \frac{1}{\tau} \log |\lambda_2(\mathcal{P}_{\tilde{s},\tilde{s}+\tau})|, \quad (25)$$

where $\lambda_2(\cdot)$ denotes the second largest eigenvalue of the argument. The maximizer of the left hand side is the eigenfunction f_s of $\mathcal{P}_{s,s+\tau}$ corresponding to this eigenvalue.

Proof. See Appendix A.7. □

The second equality in (25) states that this eigenvalue does not depend on s .

6 The generator on augmented phase space

Let us first recapitulate the developments in the last three sections. In order to have a notion of coherence with a tractable stochastic generalization, we introduced escape rates based on survivor sets in sections 3.1 and 3.2. There, the main result was Theorem 11, showing that the non-autonomous escape rate equals the autonomous escape rate of the associated augmented system. The generalization of escape rates to stochastically perturbed systems was introduced in section 4. Finally, Theorem 19 and Proposition 20 showed that coherent families can be found by considering the Lyapunov spectrum of the transfer operator family associated with the system.

Next we would like to find coherent families directly in augmented space, in a way cross-breeding theorems 11 and 19. To this end, we start with an informal reasoning to get to our main object, introduced in equation (26) below.

Recall from equations (20) and (21) that the non-homogeneous SDE $dx_t = v(t, x_t)dt + \varepsilon dw_t$ can be made homogeneous by augmenting the state space, $d\mathbf{x}_t = \mathbf{v}(\mathbf{x}_t)dt + \varepsilon d\mathbf{w}_t$. For a homogeneous process, Theorem 16 connects the escape rate from a set and the spectrum of the corresponding transfer operator semigroup. Hence, if \mathcal{P}_t denotes the transfer operator semigroup of the augmented SDE (21), then the eigenfunctions of \mathcal{P}_t yield augmented sets with low escape rates⁵. Furthermore, by the spectral mapping theorem (Proposition 15), these eigenfunctions are the same as those of the associated infinitesimal generator \mathcal{G} . The generator can be obtained from the Fokker–Planck equation associated with (21): for a scalar function \mathbf{f} , with $\mathbf{f}(\mathbf{x}) = \mathbf{f}(\theta, x)$ and “time-slices” $f_\theta := \mathbf{f}(\theta, \cdot)$, we have

$$\mathcal{G}\mathbf{f}(\theta, x) = -\partial_\theta \mathbf{f}(\theta, x) + \mathcal{G}_\theta f_\theta(x), \quad (26)$$

⁵Thus, by Proposition 14, it also yields coherent families. Here, however, we will take a different path, to add further connections shown in Figure 3, and to allow us to deal with slightly more general coherent families (recall that Theorem 16 requires closed sets). This construction will further reveal *quasi-periodic* coherent families, cf. Remark 24 below.

with domain satisfying

$$D(\mathcal{G}) \supset \{ \mathbf{f} \mid \theta \mapsto f_\theta \in C^1(\tau S^1, L^r), f_\theta \in D(\mathcal{G}_\theta) \forall \theta \in \tau S^1 \},$$

for some $1 \leq r < \infty$. We call \mathcal{G} the *augmented generator*.

Remark 21: The semigroup \mathcal{P}_t above is equivalent to the so-called *evolution semigroup*; cf. [CL99, Sch99, RSR+00, EN00] and references therein, while the idea seems to go back to [How74].

Lyapunov exponents. Our next results state that the augmented generator contains the information about the Lyapunov spectrum of the periodically driven transfer operator family; that is, it could be viewed as a spectral mapping theorem for such families of operators. In the context of evolution semigroups such results are again known by the name spectral mapping theorems (or the existence of exponential dichotomies), and can be found e.g. in [CL99] or [EN00, Section VI.9].

Lemma 22: If $\mathcal{G}\mathbf{f} = \mu\mathbf{f}$ for some $\mu \in \mathbb{C}$, then $\mathbf{f}(s+t \bmod \tau, \cdot) = e^{-\mu t} \mathcal{P}_{s,s+t} \mathbf{f}(s, \cdot)$, for $s \in \tau S^1$, $t \geq 0$. In particular, $\mathcal{P}_{s,s+\tau} f_s = e^{\mu\tau} f_s$, i.e. the time-slices of \mathbf{f} are eigenfunctions of $\mathcal{P}_{s,s+\tau}$ for the corresponding $s \in \tau S^1$.

Proof. See Appendix A.8. □

Note that since eigenfunctions of $\mathcal{P}_{s,t}$ have zero mean, we have $\int f_\theta dm = 0$ for all $\theta \in \tau S^1$. Thus, combining Lemma 22 with Proposition 20 shows that eigenfunctions of \mathcal{G} at *subdominant* eigenvalues, i.e. at eigenvalues μ where $\text{Re}(\mu)$, the real part of μ , is close to zero, yield coherent families. The following theorem shows that these eigenfunctions are exactly the same as those in the transfer operator based family arising implicitly in (25). Hence, it is an augmented time-infinitesimal version of Proposition 20.

Theorem 23: For every $s \in \tau S^1$ we have

$$\max_{f \neq 0} \Lambda_s(f) = \text{Re}(\lambda_2(\mathcal{G})) , \tag{27}$$

with $\lambda_2(\mathcal{G})$ denoting the first subdominant eigenvalue of \mathcal{G} . The s -dependent maximizer of the left-hand side is $f = \mathbf{f}(s, \cdot)$, where \mathbf{f} is the corresponding eigenfunction of \mathcal{G} .

Proof. See Appendix A.8. □

Remark 24 (The complex eigenvalue case): Suppose $\lambda_2(\mathcal{G}) =: \mu \in \mathbb{C} \setminus \mathbb{R}$. Then there is a $\delta > 0$ such that $e^{\delta\mu} \in \mathbb{R}$. For $t = s + k\delta$, $k \in \mathbb{N}$, we then have by recalling $\mathcal{P}_{s,t} f_s = e^{\mu(t-s)} f_t$ from Lemma 22, that

$$\mathcal{P}_{s,t} f_s = e^{k\delta\mu} f_t . \tag{28}$$

However, $\mathcal{P}_{s,t}$ maps real-valued functions again to real-valued ones, hence (28) holds also for the real parts $f_s^{\text{R}}, f_t^{\text{R}}$ and imaginary parts $f_s^{\text{I}}, f_t^{\text{I}}$ of f_s, f_t , respectively. The operator $\mathcal{P}_{s,t}$ is

non-expansive for *every* $s \leq t$, hence the function $t \mapsto \|\mathcal{P}_{s,t}g\|_{L^1}$ is monotonically decreasing for any g . Setting $g = f_s^{\text{R}}$ or $g = f_s^{\text{I}}$, this shows together with (28) that

$$\Lambda_s(f_s^{\text{R}}) = \Lambda_s(f_s^{\text{I}}) = \mu. \quad (29)$$

In order to obtain a coherent family in the sense of Theorem 19, we may consider the positive (or negative) support of $\mathcal{P}_{s,t}f_s^{\text{R}}$. Again from Lemma 22, we see that

$$\mathcal{P}_{s,t}f_s^{\text{R}} = \text{Re}(e^{\mu(t-s)}f_t) = e^{\alpha(t-s)}(\cos(\beta(t-s))f_t^{\text{R}} - \sin(\beta(t-s))f_t^{\text{I}}), \quad (30)$$

where $\mu = \alpha + \beta i$, $\alpha, \beta \in \mathbb{R}$ (we note that a similar construction has been employed in [FGTQ14] for the discrete time case). In particular, the real part of f_s returns to a real function f_t at some later $t = 2\pi/\beta$, where β is completely independent of the driving period τ . The corresponding coherent family of sets will be periodic if and only if τ and $\frac{2\pi}{\text{Im}(\mu)}$ are rationally dependent (i.e., they have a finite common multiple), otherwise the family will be quasi-periodic. We now show that the decision to use f^{R} represents one “phase” from a cycle of period $2\pi/\beta$.

Since the decay rate of both f_s^{R} and f_s^{I} is μ , the decay rate of any (complex) linear combination of these functions is also μ . Thus,

$$f_s^\vartheta := \text{Re}(e^{i\vartheta}f_s)$$

yields a coherent family for every $\vartheta \in [0, 2\pi)$ and ϑ acts as a *phase* for the family of coherent sets. One has the same evolution rule as in (30):

$$\mathcal{P}_{s,t}f_s^\vartheta = \text{Re}(e^{i\vartheta + \mu(t-s)}f_t).$$

Some notes on the spectrum of \mathcal{G} . The differentiation operator ∂_θ , acting on $C^1(\tau S^1)$ has the eigenfunctions $\psi_k(\theta) = \exp(2\pi i k \theta / \tau)$, $k \in \mathbb{Z}$, with corresponding eigenvalues $2\pi i k \tau^{-1}$. If \mathbf{f} is an eigenfunction of \mathcal{G} for some eigenvalue λ , then \mathbf{g} defined by $g_\theta = f_\theta \psi_k(\theta)$ is also an eigenfunction of \mathcal{G} , since

$$\begin{aligned} (\mathcal{G}\mathbf{g})(\theta, \cdot) &= \mathcal{G}_\theta g_\theta - \partial_\theta g_\theta \\ &= \underbrace{(\mathcal{G}_\theta f_\theta - \partial_\theta f_\theta)}_{=(\mathcal{G}\mathbf{f})(\theta, \cdot) = \lambda f_\theta} \psi_k(\theta) - 2\pi i k \tau^{-1} f_\theta \psi_k(\theta) \\ &= (\lambda - 2\pi i k \tau^{-1})\mathbf{g}(\theta, \cdot). \end{aligned} \quad (31)$$

Thus the point spectrum of \mathcal{G} is invariant under translation by the multiples of the scaled imaginary unit $2\pi i \tau^{-1}$. We call such translates of an eigenvalue “companion eigenvalues”. We shall also analyze in the following how this spectral property is distorted by the numerical discretization.

7 Numerical analysis

Our general strategy is going to be to solve the eigenproblem in the bottom right corner of Figure 3 numerically, and then use our results to move to the top left corner of this figure and infer quantitative information about coherent families in the system at hand.

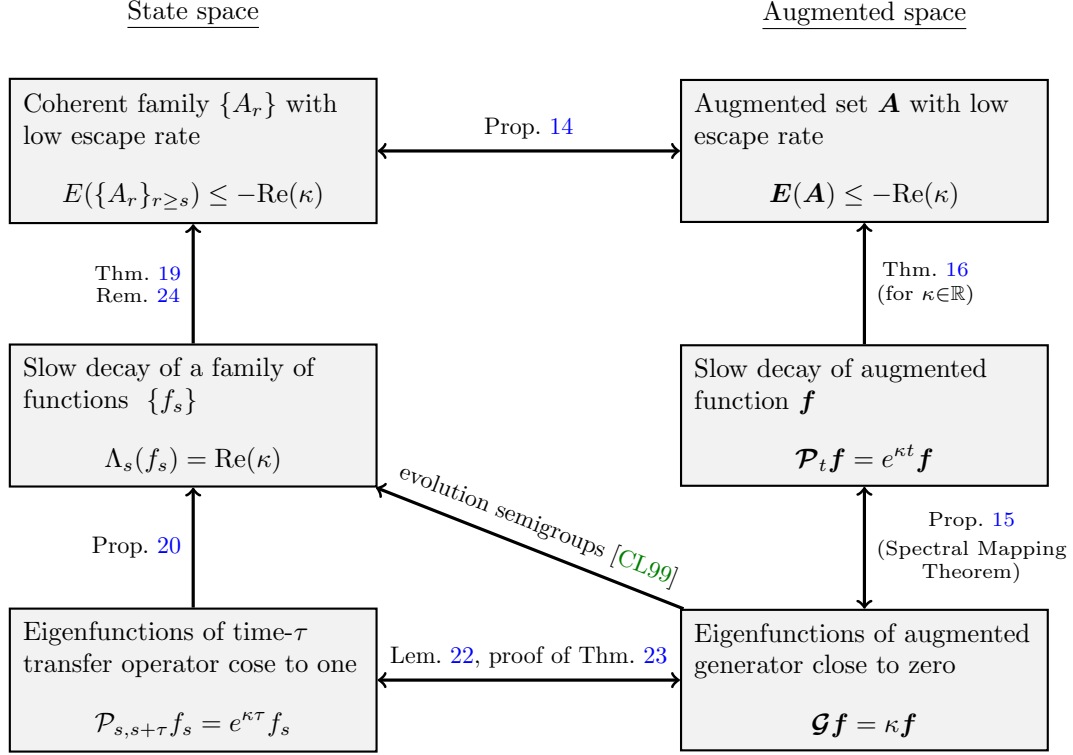


Figure 3: Connections between the different objects and concepts introduced and derived in sections 4–6. The objects on the left-hand side live in or on the state space X , while those on the right-hand side live in or on the augmented space \mathbf{X} . The arrows indicate that from the objects in the box at the tail of an arrow one can construct objects in the box at the head of that arrow. The precise statements, and the conditions under which they hold true, can be found in the main text.

7.1 Galerkin and Petrov–Galerkin methods

The Galerkin discretization of an operator \mathcal{A} over some Hilbert space \mathcal{H} with scalar product $\langle \cdot, \cdot \rangle$ can be described as follows. Suppose we have a finite-dimensional subspace $\mathcal{V} \subset \mathcal{H}$ with basis (ψ_1, \dots, ψ_k) given. The *Galerkin projection* of \mathcal{A} to \mathcal{V} is the unique linear operator $A : \mathcal{V} \rightarrow \mathcal{V}$ satisfying

$$\langle \psi_j, A\psi_i \rangle = \langle \psi_j, \mathcal{A}\psi_i \rangle, \quad \text{for all } i, j = 1 \dots, k. \quad (32)$$

If the operator \mathcal{A} is not given on a Hilbert space, just a Banach space, or for computational reasons, it can be advantageous to take *basis functions* (with respect to which the projected operator is defined) and *test functions* (which serve in (32) to project objects not necessarily living in the same subspace) from different sets.

If $\mathcal{A} : \mathcal{X} \rightarrow \mathcal{X}$ is an operator on a Banach space \mathcal{X} , $\mathcal{V} \subset \mathcal{X}$ a subspace with basis (ψ_1, \dots, ψ_k) , $\mathcal{V}^* \subset \mathcal{X}^*$ a subspace of the dual of \mathcal{X} with basis $(\psi_1^*, \dots, \psi_k^*)$, in particular $\dim \mathcal{V} = \dim \mathcal{V}^*$, then the *Petrov–Galerkin* projection of \mathcal{A} is the unique linear operator

$A : \mathcal{V} \rightarrow \mathcal{V}$ satisfying

$$\langle \psi_j^*, \mathcal{A}\psi_i \rangle = \langle \psi_j^*, A\psi_i \rangle, \quad \text{for all } i, j = 1, \dots, k, \quad (33)$$

where $\langle \cdot, \cdot \rangle$ denotes the duality bracket. There are two methods of special interest for us.

Ulam's method. Let the operator to project be the transfer operator $\mathcal{P}_{s,t} : L^1 \rightarrow L^1$, and suppose a partition of X into measurable sets B_1, \dots, B_n is given. Define the basis functions as the normed characteristic functions over the B_i , that is, $\psi_i = m(B_i)^{-1} \mathbb{1}_{B_i}$. Since thus $\psi_i \in L^\infty$, we can take $\psi_i^*(f) = \int f \psi_i$, and the corresponding Petrov–Galerkin projection of $\mathcal{P}_{s,t}$, denoted by $P_n(s, t) \in \mathbb{R}^{n \times n}$, is called the *Ulam discretization* of the transfer operator. Direct computation shows that

$$P_{n,ij}(s, t) = \mathbb{P}_{x_s \sim \text{unif}(B_j)}(x_t \in B_i),$$

where $\text{unif}(B)$ denotes the uniform distribution over the set B .

Collocation. If \mathcal{X} is a function space satisfying $\mathcal{X} \subset C^0(X)$, and $x_1, \dots, x_n \in X$, one can take $\psi^* = \delta(\cdot - x_j) \in C^0(\mathcal{X})^*$, the delta distributions centered at the x_j , i.e. $\langle \delta(\cdot - x_j), \psi \rangle = \psi(x_j)$. The associated projection is called *collocation*, because it satisfies

$$(A\psi)(x_i) = (\mathcal{A}\psi)(x_i) \quad \text{for all } \psi \in \mathcal{V}, \quad i = 1, \dots, n.$$

7.2 Ulam's discretization for the generator

Partition X into $\{B_1, \dots, B_n\}$, with each B_k , $k = 1, \dots, n$ closed, with piecewise smooth boundary, and nonempty interior. For simplicity, let us assume that the B_i are rectangular sets.

We have seen in section 5.1 that the transfer operator family associated with the homogeneous process which is governed by the SDE $dx_t = v(x_t)dt + \varepsilon dw_t$ is a semigroup, and hence has an infinitesimal generator. The Ulam discretization of this generator consists of two components, to be discussed in the following.

The first takes care of the deterministic part, which corresponds to the drift v . It can be seen as a discretization of the divergence term on the right hand side of the Fokker–Planck equation (22). The Ulam matrix P_n corresponding to the dynamics governed by the ordinary differential equation $\dot{x}(t) = v(x(t))$ satisfies that $P_n(s, t)$ only depends on $(t - s)$, since the system is autonomous. Let this Ulam discretization be denoted by $P_n(t)$. Note that since time evolution and discretization do not commute, in general $P_n(t + s) \neq P_n(t)P_n(s)$. Nevertheless, we define the first component of the generator matrix as

$$G_n^{\text{drift}} := \left. \frac{d}{dt} P_n(t) \right|_{t=0}. \quad (34)$$

This limit exists, and can be shown to yield⁶ [FJK13]

$$G_{n,ij}^{\text{drift}} = \begin{cases} \frac{1}{m(B_j)} \int_{\partial B_i \cap \partial B_j} \langle v(x), n_j(x) \rangle^+ d\sigma(x), & i \neq j \\ -\frac{1}{m(B_i)} \int_{\partial B_i} \langle v(x), n_i(x) \rangle^+ d\sigma(x), & i = j, \end{cases}$$

where n_j denotes the unit outer normal vector on ∂B_j . G_n^{drift} in this latter form is also known as the (spatial part of the) upwind scheme [LeV02].

The second component deals with the diffusion, hence corresponds to the term with the Laplace operator in (22). Note that if we would have involved the diffusion in the construction above, then the limit in (34) would have diverged. This is due to the non-Lipschitz nature of Brownian motion, as discussed earlier. The diffusion component is merely going to be the finite difference approximation Δ_n of the Laplace operator Δ on the grid defined by the centroids of the rectangles B_i , given by its representation with respect to the basis functions $\psi_i = \frac{1}{m(B_i)} \mathbb{1}_{B_i}$. We define the diffusion component of the generator as

$$G_n^{\text{diff}} := \frac{\varepsilon^2}{2} \Delta_n. \quad (35)$$

The discrete Ulam generator is then $G_n := G_n^{\text{drift}} + G_n^{\text{diff}}$. It can be readily seen that the matrix G_n is a *generator matrix*, meaning that $\exp(tG_n)$ is similar to a column-stochastic matrix for every $t \geq 0$. Hence, it has an eigenvalue 0, and all eigenvalues are in the left complex half plane, mimicking this property of its continuous original, the infinitesimal generator \mathcal{G} . Further properties of G_n , such as convergence to \mathcal{G} in an appropriate way, are shown in [Kol10, Section 5].

7.3 The discretized augmented generator and its spectrum

How does the numerical discretization from Section 7.2 reflect the theoretical findings (31) about the augmented generator \mathcal{G} ?

For the Ulam discretization of the augmented generator the time derivative appears as simple backward finite difference, cf. [FJK13, Corollary 4.5]. More precisely, if \mathbf{v} is a discretized function in augmented space,⁷ then let v_t , $t = 0, h, 2h, \dots, \tau - h$, denote its time slices, where $h = \tau/n$ for some $n \in \mathbb{N}$. The backward difference operator δ_t is given by $(\delta_t \mathbf{v})_t = h^{-1}(v_t - v_{t-h})$. By denoting $\omega := e^{2\pi i h/\tau}$, the eigenvectors of δ_t are the vectors $\psi_k = (1, \omega^k, \omega^{2k}, \dots, \omega^{(n-1)k})^T$, $k = 0, \dots, n-1$, with corresponding eigenvalues $\lambda_k := \frac{1-\omega^{-k}}{h}$.

Let \mathbf{G} denote the (Ulam) discretized augmented generator, and \mathbf{v} its eigenvector, such that $\mathbf{G}\mathbf{v} = \lambda\mathbf{v}$. Further, consider \mathbf{w} with $w_t = v_t \psi_k(t)$. A short computation shows that

$$(\mathbf{G}\mathbf{w})_t = \lambda w_t + \frac{\omega^{-k} - 1}{h} v_{t-h} \psi_k(t) = \lambda w_t - \lambda_k v_{t-h} \psi_k(t), \quad (36)$$

⁶In [FJK13], the matrix representation of the discrete generator was given with respect to the basis functions $\psi_i = \mathbb{1}_{B_i}$, here we give it with respect to the basis functions $\psi_i = \frac{1}{m(B_i)} \mathbb{1}_{B_i}$. Note also, that our matrix representations act by multiplication from the left, i.e. $f \mapsto G_n f$ for $f \in \mathbb{R}^n$.

⁷In this section we are not going to make any reference to the vector field, previously denoted by v . We use v for a different object here.

which can be seen as a discrete analogue to (31), as for $h \rightarrow 0$ we have $\frac{\omega^{-k}-1}{h} \rightarrow -2\pi ik/\tau$. Note the time shift in \mathbf{v} occurring in (36). If h is small and v_t sufficiently smooth (in t), then (36) shows that \mathbf{w} is close to being an eigenvector at $\lambda - \lambda_k$, since $v_t \approx v_{t-h}$.

If we have a discrete equivariant measure not changing in time, i.e. $G_t v_t = 0$ with $v_t = v$ for some v for all t , then the associated \mathbf{w} are indeed eigenfunctions of \mathbf{G} at $\lambda - \lambda_k$. This is the case e.g. for divergence-free non-autonomous vector fields, where the constant density is stationary. This property is inherited by Ulam's discretization of the generator, since by Gauß' theorem the total inward and outward fluxes cancel out on the boundary of every set B_i , and thus the constant vector is in the null space of the discrete generator.

7.4 Hybrid generator

Rather than approximating the space $\tau S^1 \times X$ with a single scheme, we approximate time-dependence using Fourier modes⁸ $e^{2\pi i m t/\tau}$, $m = -(M-1)/2, \dots, (M-1)/2$; hence we arrive at a hybrid collocation-Ulam scheme. The advantages of the Fourier representation are that the time derivative is explicitly known and the space spanned by this finite set of modes is invariant under time differentiation. Moreover, if the temporal change of the vector field is sufficiently smooth, due to the spectral convergence properties of Fourier collocation we expect to obtain good results with only a few modes in time direction, i.e. very small M .

In the spatial direction we use Ulam's method for the generator [FJK13]. Partition X into $\{B_1, \dots, B_N\}$, with each B_n , $n = 1, \dots, N$, closed with piecewise smooth boundary, and nonempty interior. We allow $B_j \cap B_k$ to intersect at their common boundary. The finite-dimensional estimate of \mathcal{G}_t is an $N \times N$ matrix $G(t)$. We are interested in the projection of the augmented generator \mathcal{G} onto the space spanned by the (orthogonal) functions $\{\tilde{\psi}_{n,m}\}_{n=1, \dots, N; m=-(M-1)/2, \dots, (M-1)/2}$, with $\tilde{\psi}_{n,m}(t, x) = |B_n|^{-1} e^{2\pi i m t/\tau} \mathbb{1}_{B_n}(x)$. Note, that to avoid a clash in notation, the Lebesgue measure of some set B in this section is denoted by $|B|$.

Since we want to use collocation methods, the Fourier modes shall be represented by a different basis, which is more convenient both for the assembling of the discrete operator and for the evaluation of functions given in that basis. Let $\{\ell_m\}_{m=1, \dots, M}$ denote the *Lagrangian basis* of the subspace spanned by the Fourier modes with respect to the equidistant collocation nodes $t_l = \tau(l-1)/M$, $l = 1, \dots, M$. That is, $\ell_m(t_l) = \delta_{l,m}$, where we use the usual Kronecker notation. The basis functions with respect to which we set up our discretization is $\psi_{n,m} = |B_n|^{-1} \mathbb{1}_{B_n} \ell_m$, $n = 1, \dots, N$, $m = 1, \dots, M$.

Now, to discretize \mathcal{G} over the hybrid basis, we employ a Petrov-Galerkin method with $\psi_{k,\ell}^*(t, x) = \mathbb{1}_{B_k}(x) \delta(t - t_\ell)$, $k = 1, \dots, N$, $\ell = 1, \dots, M$. Putting all this into (33), we obtain the $(n, m), (k, l)$ -th entry of the discrete augmented generator \mathbf{G} ,

$$\mathbf{G}_{(n,m),(k,l)} = -\ell'_m(t_l) \delta_{k,n} + G(t)_{n,k} \delta_{m,l}. \quad (37)$$

The expected benefit of the hybrid scheme is that we can compute the generator(s) on X at various times instead of computing on the higher-dimensional space $\mathbf{X} = \tau S^1 \times X$. If the

⁸In order to obtain a pure real approximation of real objects, for every Fourier frequency m one has to include the mode with the frequency $-m$ too. Thus, we use an odd number of modes, M .

variation of the vector field in time is sufficiently smooth, then we expect high accuracy of the discretization already with a small number of time collocation points.

Just as in section 7.3, we can search for “companion eigenmodes” in case of our hybrid discretization (37). If \mathbf{v} is an eigenfunction of \mathbf{G} for the eigenvalue λ , then consider \mathbf{w} with $w_t = v_t \psi_k(t)$, where ψ_k was defined in section 7.3. The fact that the derivative of the functions ψ_k , $-\frac{M-1}{2} \leq k \leq \frac{M-1}{2}$, is reproduced exactly by spectral differentiation implies together with (37) that \mathbf{w} is an eigenfunction for eigenvalue $\lambda - \lambda_k$, with $\lambda_k = 2\pi i k \tau^{-1}$. This matches the analytical shift of the augmented generator, cf. (31).

7.5 Example 1: a periodically driven double gyre flow

We consider the non-autonomous system [FPG14]

$$\begin{aligned} \dot{x} &= -\pi A \sin(\pi f(t, x)) \cos(\pi y) \\ \dot{y} &= \pi A \cos(\pi f(t, x)) \sin(\pi y) \frac{df}{dx}(t, x), \end{aligned} \tag{38}$$

where $f(t, x) = \alpha \sin(\omega t)x^2 + (1 - 2\alpha \sin(\omega t))x$. We fix the parameter values $A = 0.25$, $\alpha = 0.25$ and $\omega = 2\pi$, hence the vector field has period 1. The system preserves the Lebesgue measure on $X = [0, 2] \times [0, 1]$. Explicit diffusion is added to the system (cf. (19)) with $\varepsilon = 0.1$ and reflecting boundary conditions. Equation (38) describes two counter-rotating gyres next to each other (the left one rotates clockwise), with the vertical boundary between the gyres oscillating periodically.

We consider the Ulam discretization of the augmented generator, \mathbf{G} , on a uniform $30 \times 100 \times 50$ partition of the augmented state space $\mathbf{X} = S^1 \times X$. The first couple of eigenvalues with the largest real part are (as computed in Matlab by the command `eigs(G, 11, 'LR')`)

```
-0.0000 + 0.0000i
-0.0832 + 0.0000i
-0.3160 + 1.1437i
-0.3160 - 1.1437i
-0.3663 + 0.0000i
-0.6556 + 6.2374i
-0.6556 - 6.2374i
-0.7362 + 6.2443i
-0.7362 - 6.2443i
-0.9609 + 7.3794i
-0.9609 - 7.3794i
```

Since the constant density is invariant at every time instance, we expect $-\lambda_k = -\frac{1 - \exp(-2\pi i k/30)}{1/30}$ to be an eigenvalue for every $k \in \mathbb{Z}$ with an eigenfunction which is constant in the spatial direction (cf. section 7.3). Indeed, $-\lambda_{\pm 1}$ occurs among the computed eigenvalues, they are the top two underlined eigenvalues.

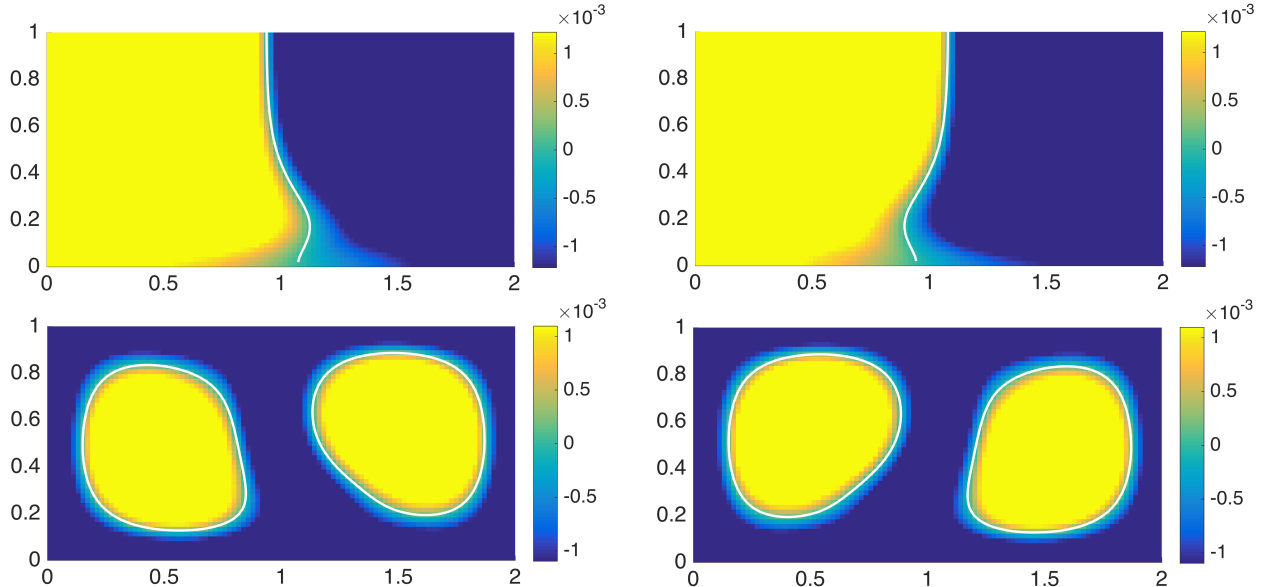


Figure 4: Time slices of the eigenvectors for the largest nonzero real eigenvalues (top: largest real eigenvalue -0.0832 , bottom: second largest real eigenvalue -0.3663) at time $t = 0$ (left) and $t = 0.5$ (right). The white contour indicates the zero-level curve.

The second eigenvalue of \mathbf{G} , about -0.0832 , indicates the most coherent family. The corresponding eigenvector \mathbf{v} is not constant in time, hence we cannot expect to find a companion eigenvalue of \mathbf{G} exactly at $-0.0832 - \lambda_{\pm 1} = -0.7388 \pm 6.2374i$, but we do anticipate an eigenvalue close by with an associated eigenvector close to $\mathbf{v}\psi_{\pm 1}$ (the multiplication is meant pointwise for the temporal components). To check this, we compute correlations between the first 20 eigenvectors \mathbf{u}_n , $n = 1, \dots, 20$, and $\mathbf{v}\psi_{\pm 1}$, i.e.

$$c_n^{\pm} = \frac{\langle \mathbf{u}_n, \mathbf{v}\psi_{\pm 1} \rangle}{\|\mathbf{u}_n\|_2 \|\mathbf{v}\psi_{\pm 1}\|_2},$$

where $\|\mathbf{u}\|_2$ is the standard Euclidean norm of the vector $\mathbf{u} \in \mathbb{R}^{30 \cdot 100 \cdot 50}$. The eigenvectors associated with the bottom two underlined eigenvalues, $-0.7362 \pm 6.2443i$, yield correlations $c_{5,6}^{\pm} \geq 0.99$, meanwhile the correlation with the other eigenfunctions does not exceed 0.02.

Figure 4 shows two time slices for the first two subdominant eigenfunctions for real eigenvalues. The top row suggests that the most coherent splitting approximately separates the left and the right gyres from one another, while the bottom row illustrates the coherence of the cores of the gyres. Note, that the zero-level curve of the dominant eigenfunction is a smoothed version of the unstable manifold of the time-independent hyperbolic fixed point $(1, 1)$ of the unperturbed flow. This observation is consistent with, but not identical to, the results in [FPG14]. There, the computations were on a finite time interval, and the boundary between the dominant finite-time coherent sets was close to the stable (resp. unstable) manifold of the hyperbolic periodic point at the initial (resp. final) time. Here,

we consider coherence over an infinite time (as in [FLS10]) and the boundaries are always approximately aligned with the *unstable* manifold of the hyperbolic periodic point.

Between the first two real subdominant eigenvalues we find a pair of complex eigenvalues, $-0.3160 \pm 1.1437i$, indicating a coherent family as well. Let \mathbf{u} be the eigenfunction for the third eigenvalue $\mu = \alpha + \beta i = -0.3160 + 1.1437i$; we extract coherent families from it, as described in Remark 24. To obtain the zero phase coherent families, we set

$$A_t^\pm = \{\pm \mathcal{P}_{0,t} u_0^{\text{Re}} \geq 0\} = \{\text{Re}(\pm e^{i\beta t} u_t) \geq 0\}.$$

Remark 24 and Theorem 19 show that the escape rate from this family is smaller than 0.3160. Figure 5 shows this coherent family at four different times. The period of the phase of the

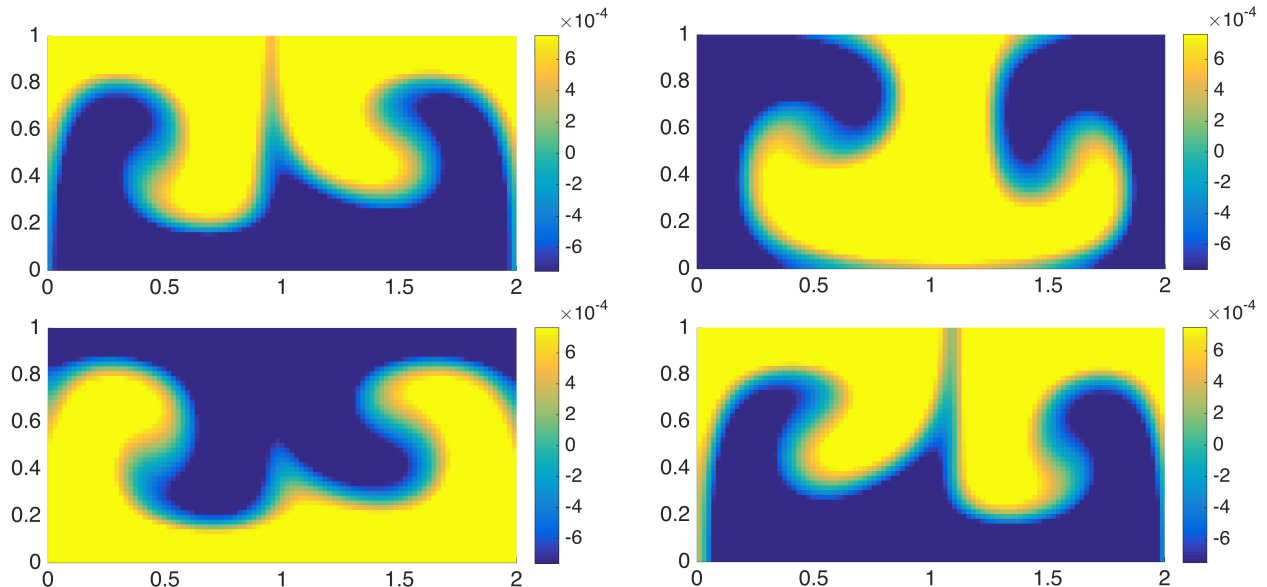


Figure 5: The functions $\text{Re}(e^{i\beta t} u_t)$, indicating the coherent families, for four different times $t = 0, 1.5, 3, 5.46$ (top left, top right, bottom left, and bottom right, respectively).

family is $2\pi/\beta \approx 5.49$, and we see in Figure 5 that after this time the coherent sets seem to have approximately completed one revolution around the centers of the gyres. This time approximately corresponds to the period of trajectories starting on the zero-level curves at the bottom of Figure 4 around the centers of the associated gyres (this is verified by numerical simulation; not shown here).

Next, we test Theorem 19 numerically. For this we choose 50000 uniformly distributed random points in X , of which 25050 lie in the positive support of the $t = 0$ slice of the eigenfunction \mathbf{v} for eigenvalue -0.0832 ; i.e. in $\{v_0 \geq 0\}$. We integrate all points from $s = 0$ to $t = 10$ (that is, 10 periods) with the Euler–Maruyama scheme (stepsize $1/30$, reflecting boundary conditions). At the end we estimate the escape rate from the family $\{A_r^\pm\}_{r \in S^1}$ by

$$\hat{E}(\{A_r^\pm\}) = -\frac{1}{t-s} \log \left(\frac{\#\text{points that stayed in } A_{r \bmod 1}^\pm \text{ for } r = 0, \frac{1}{30}, \frac{2}{30}, \dots, 10}{\#\text{points that started in } A_0^\pm} \right).$$

After averaging over five runs, we obtain $\hat{E}(\{A_r^+\}) = 0.0657$ and $\hat{E}(\{A_r^-\}) = 0.0645$, both being smaller than the associated bound by the eigenvalue $-\lambda = 0.0832$. Figure 6 shows the fraction of “surviving points” in time for different realizations of the noise process, with the theoretical bound for the slope given by the corresponding eigenvalue. Figure 7 shows the dynamical evolution of points starting in the coherent families $\{A_r^\pm\}$ for two different times.

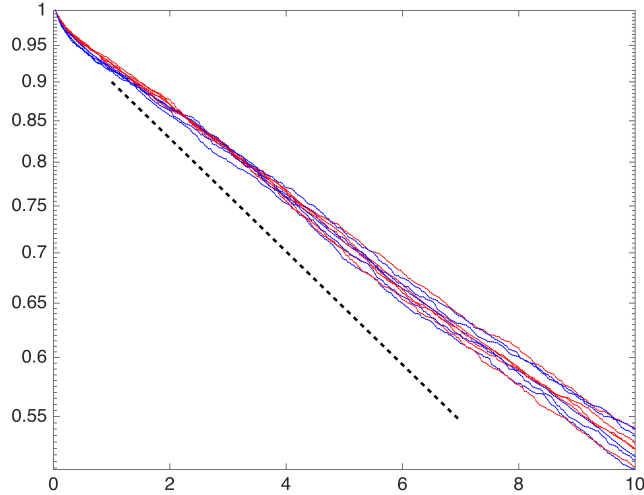


Figure 6: Numerical simulation of escape rates at anchor time $s = 0$. We show the fraction of points that stay in the coherent family until time t versus t for five test runs. Blue curves correspond to escape rates from $\{A_r^+\}$, red to those from $\{A_r^-\}$. The dashed line has slope given by the second eigenvalue.

Remark 25: In [FP09, FPG14] a line-search along different level sets is used to obtain optimal finite-time coherent sets. In the current setup we can employ a similar procedure. Recall from Theorem 2 and expression (12) that the cumulative outflow flux from the coherent family over one time period is given by the instantaneous outflow flux from the augmented set in augmented space. The entries of Ulam’s discretization of the augmented generator are exactly box-to-box instantaneous flow rates, cf. section 7.2. Hence, for any sub- or superlevel set of a given eigenfunction, the cumulative outflow flux can be computed from the discrete augmented generator \mathbf{G} in complexity that is linear in the number of boxes. Then, one would search for a level set optimizing the cumulative outflow flux to augmented volume ratio.

7.6 Example 2: periodically perturbed Bickley jet

We consider a perturbed Bickley jet as described in [RBBV⁺07]. This is an idealized zonal jet approximation in a band around a fixed latitude, assuming incompressibility, on which

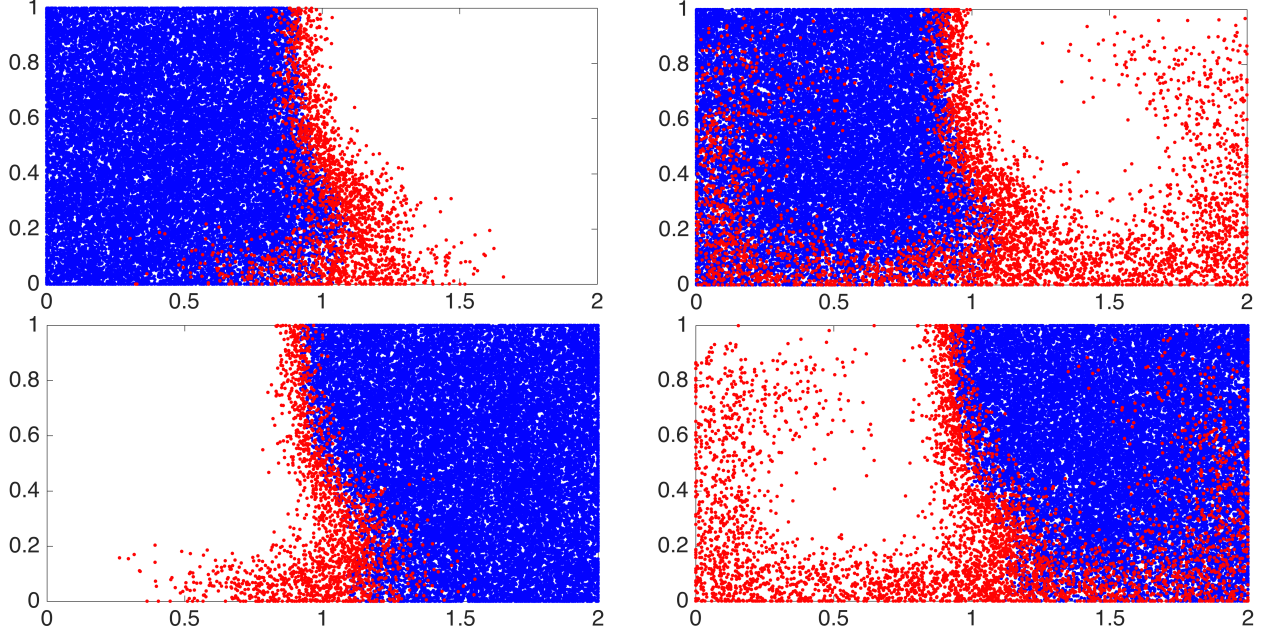


Figure 7: Numerical simulation of escape rates at anchor time $s = 0$. The points colored blue stayed in the coherent family $\{A_r^\pm\}$ for all times until time $t = 1$ (left) and $t = 3$ (right). The points that left the family at least once until time t are colored red. Top: coherent family $\{A_r^+\}$, bottom: coherent family $\{A_r^-\}$.

two traveling Rossby waves are superimposed. The dynamics is given by

$$\dot{x} = -\frac{\partial\Psi}{\partial y}, \quad \dot{y} = \frac{\partial\Psi}{\partial x},$$

with stream function

$$\Psi(t, x, y) = -U_0 L \tanh\left(\frac{y}{L}\right) + U_0 L \operatorname{sech}^2\left(\frac{y}{L}\right) \sum_{n=2}^3 A_n \cos(k_n(x - c_n t)).$$

The constants are chosen as in [RBBV+07], the length unit is Mm (1 Mm = 10^6 m), the time unit is days. Then

$$U_0 = 5.4138, \quad L = 1.77, \quad A_2 = 0.1, \quad A_3 = 0.3.$$

We set $k_n = 2n/r_e$ with $r_e = 6.371$. The phase speeds c_n of the Rossby waves are modified slightly so that the forcing is periodic with the smallest common period $\tau = 9$ days. We choose $c_2 = 0.2054 U_0$ and $c_3 = 0.4108 U_0$. The state space is periodic in the x coordinate, and is given by $X = \pi r_e S^1 \times [-4, 4]$.

Compared with our previous example, the spatial scale of dynamics is finer, and the temporal change in the vector field includes higher frequencies. Thus, we need higher resolutions for an increased accuracy, hence we employ the hybrid discretization of the augmented

generator from section 7.4 with $\varepsilon = 0.1$. We resolve time with 21 Fourier modes (such that frequencies from -10 to 10 are present), and space with a 300×120 uniform grid (resulting in almost square boxes).

Since the hybrid discretization allows for purely imaginary “companion” eigenvalues to occur by the shifts $\lambda_k = \lambda_1 k = 0.698k i$ (see the end of section 7.4), we do not compute the eigenvalues with the largest real part, but those with the smallest magnitude.⁹ Calling `eigs(G,20,'SM')` the following eigenvalues, which we order according to their real parts.

```

0.0000 + 0.0000i
-0.0138 + 0.0000i
-0.0303 + 0.0000i
-0.0332 - 0.1131i
-0.0332 + 0.1131i
-0.0333 - 0.1131i
-0.0333 + 0.1131i
-0.0443 + 0.0000i
-0.0671 - 0.0021i
-0.0671 + 0.0021i
-0.0684 - 0.0030i
-0.0684 + 0.0030i
-0.1179 + 0.0000i
-0.1322 + 0.0000i
-0.1431 - 0.1310i
-0.1703 - 0.0461i
-0.1703 + 0.0461i
-0.1703 - 0.0461i
-0.1703 + 0.0461i
-0.1864 + 0.0000i

```

By comparing the shifts with the imaginary parts of the eigenvalues, we do not expect to have any companion eigenvalues in this list. Figure 8 shows the $t = 0, 1, 2$ (top to bottom) time slices of the eigenfunctions for the framed eigenvalues. As time increases, the general pattern shown by the eigenfunctions shift from left to right. The eigenvalue bounds on the escape rates together with the corresponding eigenfunctions suggest that the least transport occurs across the meandering horizontal jet region around $y = 0$ (2nd eigenfunction, left column, Figure 8), while there is also low transport between the extreme northern/southern boundaries, coloured dark blue, and the central horizontal region, coloured yellow (3rd eigenfunction, middle column, Figure 8). We also find six coherent vortices, coloured dark blue

⁹One could ask, what happens if the real eigenvalues we are interested in have larger modulus than the smallest companion eigenvalues? This would mean $\lambda_2 < -2\pi/\tau$, and the corresponding coherence estimate would be quite miserable by yielding a survivor fraction of $e^{-2\pi} \approx 0.002$ after one time period. In both of our examples this fraction is around 0.9. Note that rescaling time does not help, because this merely multiplies both the eigenvalues of the augmented generator and the companion shifts by the same scalar with which we sped up time. We leave the computational details to the reader.

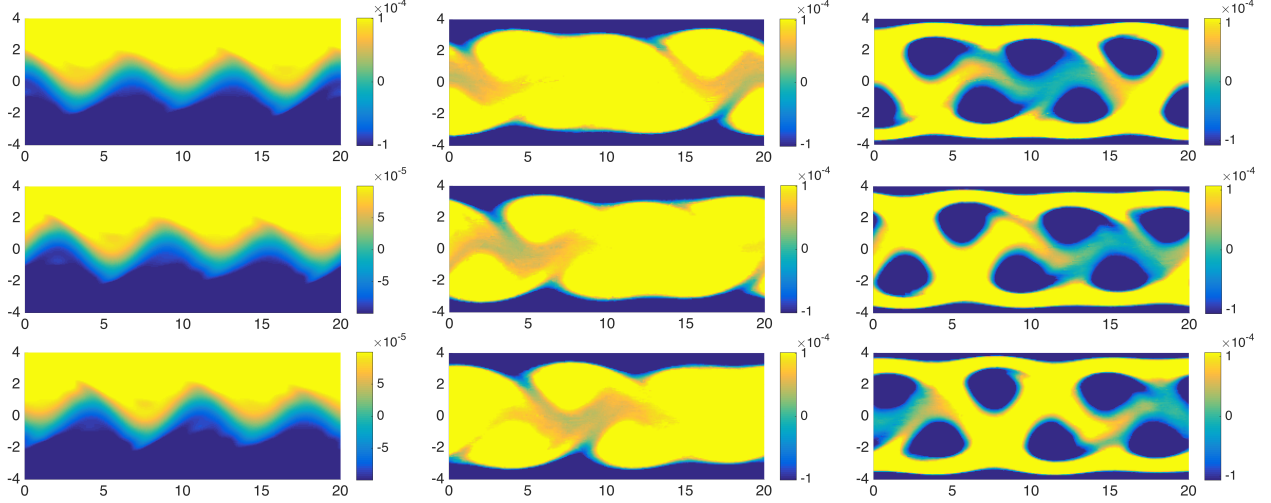


Figure 8: Eigenfunctions of the hybrid discretized augmented generator at the second, third, and thirteenth eigenvalues (left to right), shown at time slices $t = 0, 1, 2$ (top to bottom).

(13th eigenfunction, right column, Figure 8); these have a higher escape rate than the regions shown in the left and central columns of Figure 8. Sampling-based numerical simulation of the escape rate from the most coherent family (i.e. that given by the eigenfunction in the left column of Figure 8; not shown) reveals escape rates of below 0.0082, which is again overestimated by the eigenvalue bound 0.0138, consistent with the theory. Figure 9 shows the evolution of sample points starting from the top left vortex.

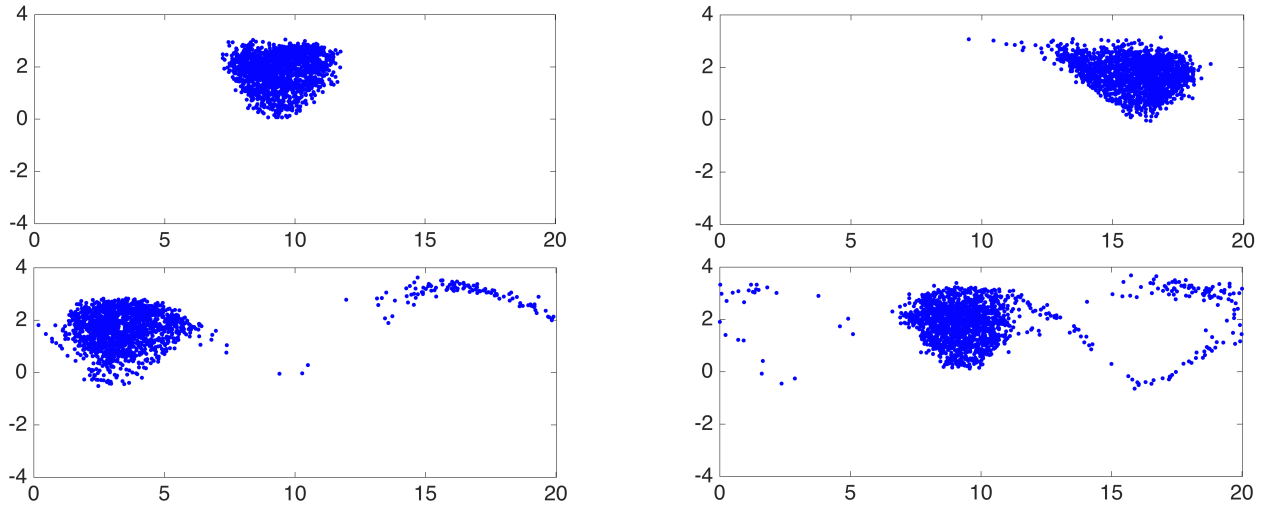


Figure 9: Evolution of sample points starting from the top left vortex (cf. the top right eigenfunction in Figure 8), shown at times $t = 3, 6, 9, 12$ (top left, top right, bottom left, and bottom right, respectively).

From the complex eigenvalues, the fourth (and fifth) and sixth (and seventh) are those which promise the most coherent sets. Since these eigenvalues are complex, we treat the

corresponding eigenfunctions as described in Remark 24. We choose the fourth eigenfunction with eigenvalue $\mu = \alpha + \beta i = -0.0332 - 0.1131i$; the sixth gives a similar but translated structure. We denote the corresponding eigenfunction by \mathbf{f} , and Remark 24 tells us that

$$A_t^\pm = \{\pm \mathcal{P}_{0,t} f_0^{\text{Re}} \geq 0\} = \{\text{Re}(e^{i\beta t} f_t) \geq 0\}$$

are coherent families. The left column of Figure 10 depicts the functions f_0^{Re} , $\mathcal{P}_{0,3} f_0^{\text{Re}}$, and $\mathcal{P}_{0,6} f_0^{\text{Re}}$. This shows us that the coherent northern and southern boundaries of the state space (already shown in Figure 8, middle column) decompose into “coherent tongues”, which move slowly from left to right. The phase repeats every $2\pi/0.1131 \approx 55.55$ days, much longer than the driving period of 9 days. Because 55.55 is not a multiple of 9, when the phase restarts, the driving will already be part way through its cycle. The spatial structures approximately return to the same x -position after 55.55 days.

The right column of this figure shows a numerical simulation of the escape from the family $\{A_t^+\}_{t \geq 0}$. In order not to pick points from the central horizontal region where \mathbf{f} is orders of magnitude smaller than its mean modulus, we initialize trajectories only where $f_0^{\text{Re}} \geq 3 \cdot 10^{-4}$.

7.7 Numerical comparison with Ulam’s method

In this section we compare the results of the augmented generator method for the periodically driven double gyre, obtained in section 7.5, with the “standard” Ulam’s method, as described in section 7.1.

To this end we assemble the Ulam matrix $P_n(s, t)$ in the usual way: via sampling-based approximation of its entries. Let us recall that Lemma 22 gives us an analytic connection between the augmented generator \mathcal{G} and the one-period transfer operator $\mathcal{P}_{s, s+\tau}$. Thus, we will consider the Ulam approximation of this transfer operator, $P = P_n(0, 1)$ (we omit the discretization subscript, and the times, since these will be fixed throughout this section).

In order to obtain results comparable with our previous ones, we discretize the state space $X = [0, 2] \times [0, 1]$ uniformly into 100×50 boxes. The *transition rates* between the boxes, i.e. the entries of the matrix P ,

$$P_{ij} = \mathbb{P}_{x_s \sim \text{unif}(B_j)}(x_t \in B_i),$$

are computed via sampling. For every box B_j we choose $N = 2500$ random test points¹⁰ $x_s^{(1)}, x_s^{(2)}, \dots, x_s^{(N)}$ at the initial time, and we set

$$P_{ij} = \frac{1}{N} \sum_{k=1}^N \mathbb{1}_{B_i}(x_t^{(k)}),$$

¹⁰For comparison, in [FPG14], the finite-time (as opposed to infinite-time in the present study) coherent set experiments for the double gyre used a grid of 128×64 boxes and 10000 points per box. These 10000 points comprised 400 uniformly distributed points per box, and each of these 400 points had an associated 25 points describing an ϵ -ball neighbourhood ($\epsilon = 0.02$). Then, these points were integrated with a fourth-order Runge–Kutta scheme with constant stepsize 0.01 for a time span of length 1, resulting in a total number of vector field evaluation about $8 \cdot 10^9$. This procedure approximates a deterministic flow of 1 period, followed by uniform noise in an ϵ -ball. In the present paper we instead simulate an SDE for 1 period.

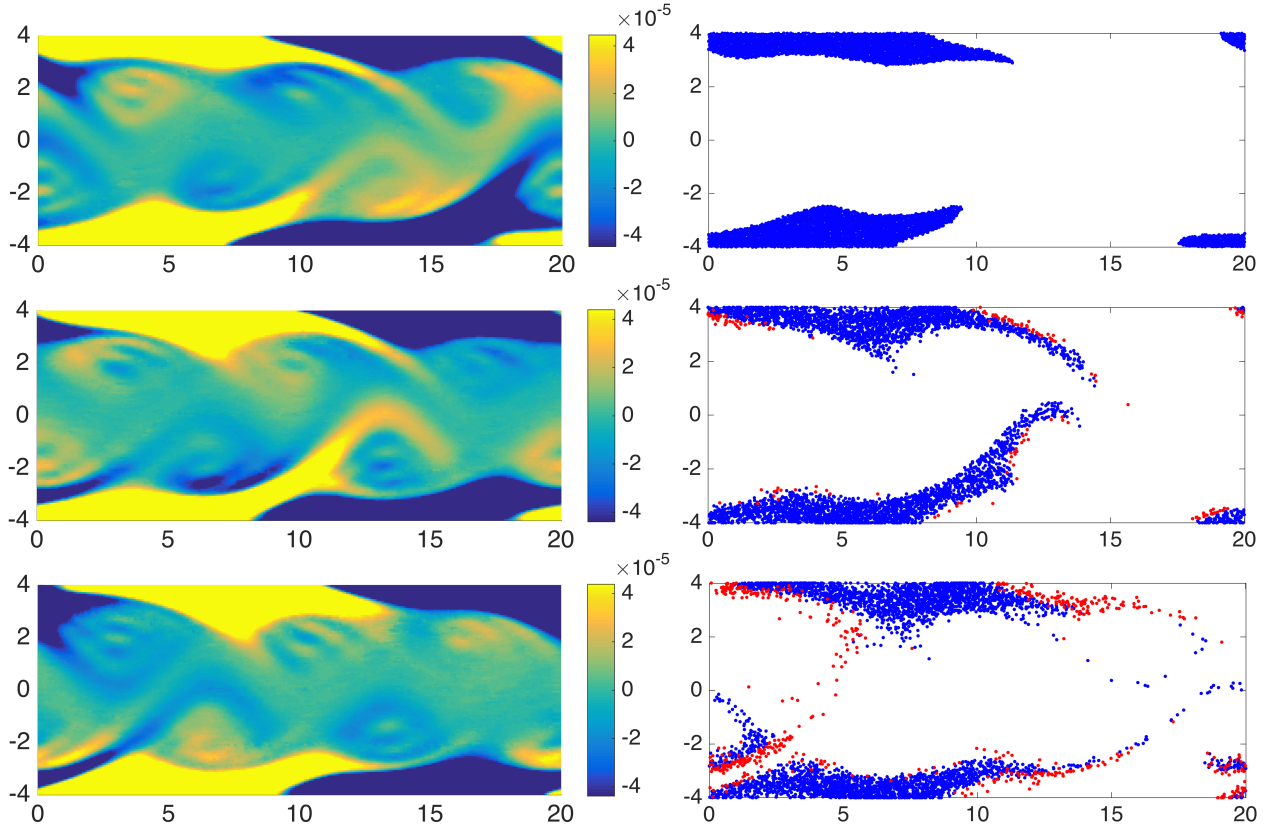


Figure 10: Left: real part of the $s = 0$ time slice of the ninth eigenfunction of the hybrid discretized augmented generator evolved to times $t = 0, 3, 6$ (top to bottom). Right: escape rate simulation; trajectories shown at the corresponding times. The blue points stayed in the coherent family until the time when they are shown, the red ones have left the family prior to this time.

where $x_t^{(k)}$, $k = 1, \dots, N$, are independent realizations of the underlying stochastic process computed by the Euler–Maruyama method [KP92] (with reflecting boundary) for step-size $1/30$ (the temporal direction was also discretized in 30 boxes in section 7.5). Note that this leads to $375 \cdot 10^6$ evaluations of the vector field, a factor 25 times more than in the case of the augmented generator, where we used a two-dimensional Gauß quadrature with 4×4 nodes on each of the 6 faces of the three-dimensional boxes. Note that since the augmented vector field is constant in the temporal direction, we could calculate the transition rates in this direction analytically, thus effectively reducing the need for quadrature to 4 from the 6 faces. Even larger savings can be obtained by applying the hybrid discretization from section 7.4: not only can we work with lower temporal resolutions, but also the generators $G(t)$ in (37) are computed on the lower-dimensional space X instead of \mathbf{X} .

We expect the dominant eigenvalues and eigenfunctions of P to be associated with the eigenvalues and eigenfunctions of the augmented generator \mathbf{G} , predicted by Lemma 22 in the analytical case. The eigenvalues with the largest modulus are shown in Table 1, together

with their logarithmic transforms, and the corresponding eigenvalues of the augmented generator \mathbf{G} . The upwind type spatial discretization introduces so-called numerical diffusion

λ_i	$\tau^{-1} \log(\lambda_i)$	μ_i
1.0000 + 0.0000i	0.0000 + 0.0000i	-0.0000 + 0.0000i
0.9150 + 0.0000i	-0.0888 + 0.0000i	-0.0832 + 0.0000i
0.3993 + 0.6678i	-0.2509 + 1.0319i	-0.3160 + 1.1437i
0.3993 - 0.6678i	-0.2509 - 1.0319i	-0.3160 - 1.1437i
0.7616 + 0.0000i	-0.2723 + 0.0000i	-0.3663 + 0.0000i
0.6929 + 0.0000i	-0.3669 + 0.0000i	-0.5169 + 0.0000i

Table 1: Left column: dominant eigenvalues λ_i of the Ulam matrix P . Middle column: logarithms of the λ_i . Right column: corresponding eigenvalues μ_i of the Ulam discretization \mathbf{G} of the augmented generator.

in $\mathbf{G}^{\text{drift}}$ (as discussed in [FJK13]), adding to the mixing in the system.¹¹ This is the reason for the augmented generator having eigenvalues (from the third on) with smaller real parts than the corresponding log-transformed eigenvalues of the Ulam matrix. Figure 11 shows the second, third, and fifth eigenfunctions of P . All the eigenfunctions are, as expected,

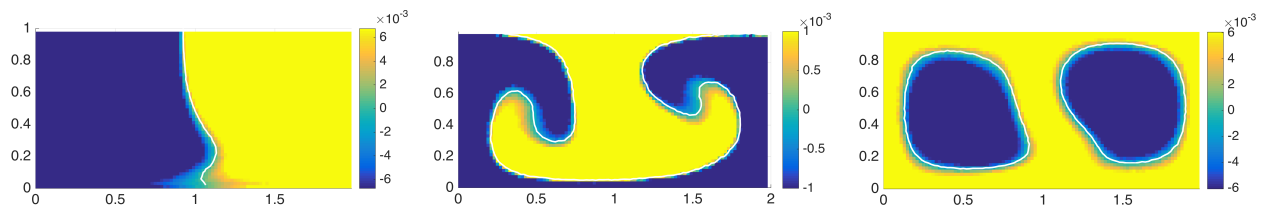


Figure 11: From left to right: second, third (shown is the real part), and fifth eigenfunctions of the Ulam discretization P of the transfer operator. The white contours indicate the zero-level curves.

very close to those of the augmented generator \mathbf{G} ; cf. Figures 4 and 5. The third, complex eigenfunction differs only in the phase, which is arbitrary. If we repeat the computation now only with 100 sample points per box, such that the overall number of vector field evaluations matches that for the augmented generator, we obtain the eigenfunctions given in Figure 12. Note that the smoothness of the numerical eigenfunctions has deteriorated due to an insufficient sampling; the zero-level curves have also lost smoothness. In general, the longer the time span (s, t) , the more sampling points have to be integrated in order to resolve the noise sufficiently, due to exponential expansion in the flow. Certainly, a larger time span

¹¹We conjecture that the second eigenvalue of \mathbf{G} , -0.0832 , is not smaller than the log-transform of the corresponding eigenvalue of P , because (i) the zero-level curve of the corresponding eigenfunction has a significant vertical component, and (ii) the vector field is approximately vertical near the zero-level curve. This likely leads to a reduction in numerical diffusion in $\mathbf{G}^{\text{drift}}$ across the zero-level curve, when compared to lower eigenvalues, since numerical diffusion occurs locally, where the vector field has a significant component transversal to a box face.

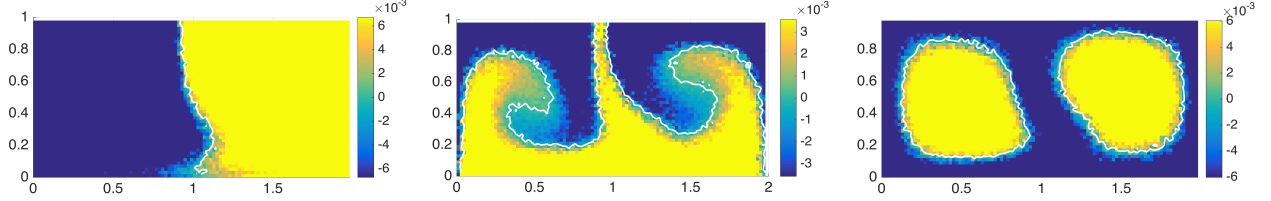


Figure 12: From left to right: second, third (shown is the real part), and fifth eigenfunctions of the Ulam discretization P of the transfer operator, now computed with a 25 times smaller number of sample points as those in Figure 11. The white contours indicate the zero-level curves.

necessitates a larger number of basis functions in the temporal direction for the augmented generator too. It is not yet clear whether this number also scales exponentially in time, or a linear growth is sufficient to maintain the same level of accuracy. The augmented generator incorporates diffusion as an additive differential operator, and guarantees for smoothness of the results.

Acknowledgments

GF is supported by an ARC Future Fellowship. PK thanks the UNSW School of Mathematics and Statistics for hospitality at an early stage of this work, and an ARC Discovery Project for supporting this visit. The authors thank Michael Kratzer for helpful comments regarding the proof of Lemma 26, Roland Schnaubelt for pointing out useful references, and Martin Plonka for his careful proofreading.

A Proofs

A.1 Proof of Theorem 2

Proof of Theorem 2. Let $D_t a$ and $D_r a$ denote the derivatives of the parametrizing function a with respect to $t \in \tau S^1$ and $r \in R$, respectively. Then, we have for the accumulated outflow flux:

$$\begin{aligned} \int_{\tau S^1} \int_{\partial A_t} \langle v(t, x) - w(t, x), n_t(x) \rangle^+ d\sigma(x) dt &= \\ &= \int_{\tau S^1} \int_R \langle v(t, a(t, r)) - D_t a(t, r), n_t(a(t, r)) \rangle^+ g_t(r) dr dt, \end{aligned} \quad (39)$$

where $g_t(r) = \det(D_r a(t, r)^T D_r a(t, r))^{1/2}$ is the Gram determinant. The outer normal in the augmented space has the form

$$\mathbf{n}(t, r) := \mathbf{n}(\mathbf{x}) = \begin{pmatrix} \alpha \\ \beta n_t(a(t, r)) \end{pmatrix},$$

with $\alpha, \beta \in \mathbb{R}$ satisfying $\alpha^2 + \beta^2 = 1$ and

$$\mathbf{n}(t, r) \perp \begin{pmatrix} 1 \\ D_t a(t, r) \end{pmatrix}.$$

Solving for \mathbf{n} yields

$$\mathbf{n}(t, r) = (1 + \langle n_t(a(t, r)), D_t a(t, r) \rangle)^{-1/2} \begin{pmatrix} -\langle n_t(a(t, r)), D_t a(t, r) \rangle \\ n_t(a(t, r)) \end{pmatrix}.$$

The instantaneous outflow flux in augmented space, $\int_{\partial \mathbf{A}} \langle \mathbf{v}(\mathbf{x}), \mathbf{n}(\mathbf{x}) \rangle^+ d\sigma(\mathbf{x})$, now reads as

$$\int_{\tau S^1 \times R} \left\langle \begin{pmatrix} 1 \\ v(t, a(t, r)) \end{pmatrix}, \begin{pmatrix} -\langle n_t(a(t, r)), D_t a(t, r) \rangle \\ n_t(a(t, r)) \end{pmatrix} \right\rangle^+ \times \\ \times \frac{\mathbf{g}(t, r)}{(1 + \langle n_t(a(t, r)), D_t a(t, r) \rangle)^2} d(t, r), \quad (40)$$

with $\mathbf{g}(t, r) = \det(D_{(t,r)} a(t, r)^T D_{(t,r)} a(t, r))^{1/2}$, where $D_{(t,r)} a$ denotes the total derivative of a with respect to the joint variable (t, r) ; i.e. $D_{(t,r)} a = (D_t a, D_r a)$. Comparing (39) with (40) shows that they are equal if and only if

$$(1 + \langle n_t(a(t, r)), D_t a(t, r) \rangle)^2 g_t(r) = \mathbf{g}(t, r) \quad \text{for every } t \in S^1, r \in R. \quad (41)$$

Using Lemma 26 below with $M = D_r a(t, r)$, $m = D_t a(t, r)$ and $n = n_t(a(t, r))$ proves (41) and completes the proof of (13).

Now that we have shown equality in (13), the independence of its left- and right-hand sides on the parametrization a is a simple corollary of the independence of surface integrals on parametrization. In particular, the right-hand side of (13), $\int_{\partial \mathbf{A}} \langle \mathbf{v}(\mathbf{x}), \mathbf{n}(\mathbf{x}) \rangle^+ d\sigma(\mathbf{x})$, is a surface integral, and hence depends only on \mathbf{v} and \mathbf{A} , and both these objects are parametrization-independent. \square

Lemma 26: Let $M \in \mathbb{R}^{k \times k-1}$ have full rank, let $n \in \mathbb{R}^k$ with $n^T M = 0$ and $n^T n = 1$, and let $m \in \mathbb{R}^k$. Then we have

$$(1 + (n^T m)^2) \det(M^T M) = \det \begin{pmatrix} 1 + m^T m & m^T M \\ M^T m & M^T M \end{pmatrix}.$$

Proof. Note that

$$\begin{pmatrix} 1 + m^T m & m^T M \\ M^T m & M^T M \end{pmatrix} = \begin{pmatrix} 1 & m^T \\ 0 & M^T \end{pmatrix} \begin{pmatrix} 1 & 0 \\ m & M \end{pmatrix}.$$

Our strategy will be to use a transformation matrix which has determinant one and changes the m on the off-diagonal blocks in the factors to a multiple of n . This will impose in the product a zero off-diagonal block, since $n^T M = 0$. Hence, let $u \in \mathbb{R}^{k-1}$ be such that

$Mu + m = (n^T m)n$. This is possible since M has full rank and by $n^T M = 0$ it holds $\text{Range}(M)^\perp = \mathbb{R}n$. Define $A := \begin{pmatrix} 1 & 0 \\ u & I_{k-1 \times k-1} \end{pmatrix}$, and note $\det(A) = 1$. By this,

$$\begin{aligned} \det \left(\begin{pmatrix} 1 & m^T \\ 0 & M^T \end{pmatrix} \begin{pmatrix} 1 & 0 \\ m & M \end{pmatrix} \right) &= \det \left(A^T \begin{pmatrix} 1 & m^T \\ 0 & M^T \end{pmatrix} \begin{pmatrix} 1 & 0 \\ m & M \end{pmatrix} A \right) \\ &= \det \left(\begin{pmatrix} 1 & (n^T m)n^T \\ 0 & M^T \end{pmatrix} \begin{pmatrix} 1 & 0 \\ (n^T m)n & M \end{pmatrix} \right) \\ &= \det \begin{pmatrix} 1 + (n^T m)^2 & 0 \\ 0 & M^T M \end{pmatrix} \\ &= (1 + (n^T m)^2) \det(M^T M). \end{aligned}$$

□

A.2 Proof of Proposition 5

Clearly, $A_{s,t} \subseteq A^n := \bigcap_{i=1}^n \phi_{r_i,s} A_{r_i}$, and $A^{n+1} \subseteq A^n$. We show that¹² $A^n \downarrow A_{s,t}$. Let us fix some $x \in X$. Note that since the sets A_r are closed, we have

$$x \notin A_{s,t} \Leftrightarrow \exists r_* : x \notin \phi_{r_*,s} A_{r_*} \Leftrightarrow d(x, \phi_{r_*,s} A_{r_*}) \geq \epsilon \text{ for some } \epsilon > 0.$$

Due to property (b) of the niceness, the function $r \mapsto d(x, \phi_{r,s} A_r)$ is continuous, hence there is a $\delta > 0$ such that $d(x, \phi_{r,s} A_r) > \epsilon/2$ for all $r \in (r_* - \delta, r_* + \delta)$. Then, there is an $N \geq 1$ such that $\{r_1, \dots, r_n\} \cap (r_* - \delta, r_* + \delta) \neq \emptyset$ for every $n \geq N$, hence

$$x \notin \bigcap_{i=1}^n \phi_{r_i,s} A_{r_i} = A^n.$$

Thus, $A^n \downarrow A_{s,t}$ as $n \rightarrow \infty$. As $A_{s,t}$ is a countable intersection of measurable sets, is is measurable itself.

By the nestedness of the A^n , i.e. $A^{n+1} \subseteq A^n$ for $n \geq 1$, and the σ -additivity of m we have

$$\begin{aligned} m(A_{s,t}) &= m(A^1) - \sum_{n=1}^{\infty} m(A^n \setminus A^{n+1}) \\ &= \lim_{k \rightarrow \infty} \left(m(A^1) - \sum_{n=1}^{k-1} m(A^n \setminus A^{n+1}) \right) \\ &= \lim_{k \rightarrow \infty} m(A^k). \end{aligned}$$

¹²For a sequence of sets $(A^n)_{n \in \mathbb{N}}$ and a set A we write $A^n \downarrow A$, if $A^{n+1} \subseteq A^n$ for every $n \in \mathbb{N}$, and $\bigcap_{n \in \mathbb{N}} A^n = A$.

A.3 Proof of Theorem 10

We begin with a lemma.

Lemma 27: Let $\varphi : X \rightarrow X$ be a diffeomorphism on a compact set X . For every measurable $A \subset X$ one has

$$|D\varphi|_{\min} m(A) \leq m(\varphi(A)) \leq |D\varphi|_{\max} m(A),$$

where $0 < |D\varphi|_{\min} = \min_{x \in X} |\det D\varphi(x)|$, and $|D\varphi|_{\max} = \max_{x \in X} |\det D\varphi(x)| < \infty$.

Proof. Note that since φ is a diffeomorphism, φ^{-1} is a continuous map, hence $\varphi(A)$ is a measurable set. By the integral transformation theorem

$$m(\varphi(A)) = \int_{\varphi(A)} 1 \, dx = \int_A 1 |\det D\varphi(x)| \, dx,$$

from which the inequalities follow immediately. Since φ is a diffeomorphism, $D\varphi$ is continuous and everywhere nonsingular, hence by the compactness of X the continuous function $|\det(D\varphi)|$, which is bounded away from zero, attains its min, which is positive, and its max, which is finite. \square

Next, by splitting the intersection, we obtain for $s_1 \leq s_2 \leq t$

$$\bigcap_{r=s_1}^t \phi_{r,s_1} A_r = \left(\bigcap_{r=s_1}^{s_2} \phi_{r,s_1} A_r \right) \cap \left(\phi_{s_2,s_1} \bigcap_{r=s_2}^t \phi_{r,s_2} A_r \right),$$

which reads in our shorthand notation as

$$A_{s_1,t} = A_{s_1,s_2} \cap \phi_{s_2,s_1} A_{s_2,t}. \quad (42)$$

This implies

$$m(A_{s_1,t}) \leq \min \{m(A_{s_1,s_2}), m(\phi_{s_2,s_1} A_{s_2,t})\} \leq m(\phi_{s_2,s_1} A_{s_2,t}). \quad (43)$$

Using continuity of the vector field v over $\tau S^1 \times X$ we have that ϕ_{s_2,s_1} is a diffeomorphism for every $s_2 \geq s_1$, and $|\det D\phi_{s_2,s_1}|$ is continuous in s_1, s_2 . Hence there are $J_{\min} > 0$ and $J_{\max} < \infty$ such that $J_{\min} \leq |\det D\phi_{s_2,s_1}(x)| \leq J_{\max} < \infty$ for every $s_1, s_2 \in \mathbb{R}/\tau\mathbb{Z}$ and $x \in X$. Lemma 27 with (43) yields

Corollary 28: For $s_1 \leq s_2 \leq t$ we have

$$m(A_{s_1,t}) \leq J_{\max} m(A_{s_2,t}).$$

Due to the monotonicity of the logarithm this corollary yields

$$\log m(A_{s_1,t}) \leq \log J_{\max} + \log m(A_{s_2,t}).$$

Taking the $-\limsup_{t \rightarrow \infty} \frac{1}{t}$ of both sides, we obtain

$$E(\{A_r\}_{r \geq s_1}) \geq E(\{A_r\}_{r \geq s_2}), \quad \text{for all } s_1 \leq s_2. \quad (44)$$

Observe that due to periodicity $E(\{A_r\}_{r \geq s}) = E(\{A_r\}_{r \geq s+\tau})$, since for $t \geq s + \tau$ one has

$$\bigcap_{r=s+\tau}^t \phi_{r,s+\tau} A_r = \bigcap_{r=s}^{t-\tau} \phi_{r+\tau,s+\tau} A_{r+\tau} = \bigcap_{r=s}^{t-\tau} \phi_{r,s} A_r,$$

the first equation resulting from a change of variable $r \rightarrow r + \tau$, while the second one coming from periodicity of both the vector field and the family of sets. With this we have from (44) that

$$E(\{A_r\}_{r \geq s_1}) \geq E(\{A_r\}_{r \geq s_2+\tau}) = E(\{A_r\}_{r \geq s_2}), \quad \text{for all } s_2 \leq s_1 \leq s_2 + \tau. \quad (45)$$

Equations (44) and (45) together yield Theorem 10.

A.4 Proof of Theorem 11

Recall the identity (17). From this we have

$$m \left(\bigcap_{s=0}^t \phi_{-s} \mathbf{A} \right) = \int_0^\tau m(A_{s,s+t}) ds.$$

Using Corollary 28 twice gives

$$\tau J_{\max}^{-1} m(A_{0,s+t}) \leq \int_0^\tau m(A_{s,s+t}) ds \leq \tau J_{\max} m(A_{\tau,s+t})$$

for sufficiently large t . Taking the $-\limsup_{t \rightarrow \infty} \frac{1}{t} \log$ of both sides and using Theorem 10 yields the claim.

A.5 Proof of Theorem 16

Fix $t > 0$ and let $(r_i)_{i \in \mathbb{N}}$ be a dense sequence in $[0, t]$ such that $r_1 = t$; this latter condition is needed such that a decomposition as in (46) is always possible. Further, define the signed measure ν via $d\nu(x) = f(x) dm(x)$.

We consider the events

$$\mathcal{E}_n := \{\omega \mid x_{r_i}(\omega) \in A^+, \forall i = 1, \dots, n\}.$$

As in the proof of Proposition 5, the continuity of sample paths and the closedness of A^+ implies $\mathcal{E}_n \downarrow \mathcal{E} := \bigcap_{r \in [0, t]} \{\omega \mid x_r(\omega) \in A^+\}$, hence the measurability of \mathcal{E} . The very same proof yields also $\mathbb{P}_\nu(\mathcal{E}_n) \rightarrow \mathbb{P}_\nu(\mathcal{E})$ as $n \rightarrow \infty$; where $\mathbb{P}_\nu = \mathbb{P}_{\nu^+} - \mathbb{P}_{\nu^-}$.

Note that since $\lambda < 0$, one has $\int f dm = 0$, hence we can take f such that $\int f^+ dm = \int_{A^+} f dm = 1$. It follows that for every $n \in \mathbb{N}$ we have [FJK13]

$$\begin{aligned}
e^{\lambda t} &= e^{\lambda t} \int_{A^+} f dm \\
&= \int_{A^+} \mathcal{P}_t f \\
&= \mathbb{P}_\nu(x_t \in A^+) \\
&= \mathbb{P}_\nu(x_{r_i} \in A^+, i = 1, \dots, n) + \underbrace{\sum_{j=2}^n \mathbb{P}_\nu(x_{r_j} \notin A^+, x_{r_i} \in A^+, \forall r_i > r_j)}_{=: p_j}. \quad (46)
\end{aligned}$$

The last equality follows from the decomposition of the event $\{x_{r_1} \in A^+\} = \{x_t \in A^+\}$ into disjoint events $\{x_{r_i} \in A^+ \text{ for all } r_i > r_j, \text{ but } x_{r_j} \notin A^+\}$, $j = 2, \dots, n$, and $\{x_{r_i} \in A^+ \text{ for all } i = 1, \dots, n\}$. One can show [FJK13] that $p_j \leq 0$, because the set of initial conditions $x_{r_j} \notin A^+$ is contained in the non-positive support of ν . It follows that

$$e^{\lambda t} \leq \mathbb{P}_\nu(x_{r_i} \in A^+, i = 1, \dots, n) = \mathbb{P}_\nu(\mathcal{E}_n). \quad (47)$$

Thus,

$$e^{\lambda t} \leq \lim_{n \rightarrow \infty} \mathbb{P}_\nu(\mathcal{E}_n) = \mathbb{P}_\nu(\mathcal{E}).$$

From now on, the proof follows the lines of [FS10, FS13]. Noting that $\mathbb{P}_\nu(\cdot) \leq \|f\|_{L^\infty} \mathbb{P}_m(\cdot)$, we obtain for every $t > 0$ that

$$\frac{1}{t} \log e^{\lambda t} \leq \frac{1}{t} \log \mathbb{P}_\nu(\mathcal{E}) \leq \frac{1}{t} (\log \mathbb{P}_m(\mathcal{E}) + \log \|f\|_{L^\infty}).$$

Taking the $-\limsup_{t \rightarrow \infty}$ of both sides we conclude the proof.

A.6 Proof of Theorem 19

The proof follows the lines of that of Theorem 16 (Appendix A.5). For a fixed $t > s$ and a sequence $(r_i)_{i \in \mathbb{N}}$, dense in $[s, t]$ and satisfying $r_1 = t$, we consider the events

$$\mathcal{E}_n := \{\omega \mid x_{r_i}(\omega) \in A_{r_i}^+, \forall i = 1, \dots, n\}.$$

The sufficient niceness of the family $\{A_r\}$ means by Definition 17 (ii), in particular, that the A_r^+ are closed and either left- or right-continuous in r , thus one can show that $\mathcal{E}_n \downarrow \mathcal{E} := \{\omega \mid x_r(\omega) \in A_r^+, \forall r \in [s, t]\}$.

Since $\mathcal{P}_{s,t}$ is a Markov operator (positive and integral preserving), we have $\int \mathcal{P}_{s,t} f = 0$ due to $\int f = 0$, and hence $\frac{1}{2} \|\mathcal{P}_{s,t} f\|_1 = \int_{A_t^+} \mathcal{P}_{s,t} f$. Let ν be the signed measure with $d\nu = f dm$, and for the ease of notation denote $\mathbb{P}_{x_s \sim \nu}(\cdot)$ by $\mathbb{P}_\nu(\cdot)$. Then we obtain in an analogous manner as above, that

$$\frac{1}{2} \|\mathcal{P}_{s,t} f\|_1 = \int_{A_t^+} \mathcal{P}_{s,t} f = \mathbb{P}_\nu(x_t \in A_t^+) \leq \mathbb{P}_\nu(\mathcal{E}_n) \xrightarrow{n \rightarrow \infty} \mathbb{P}_\nu(\mathcal{E}) \quad (48)$$

As $f \in L^\infty$, it follows by the monotonicity of the logarithm that

$$\begin{aligned}\Lambda_s(f) &= \limsup_{t \rightarrow \infty} \frac{1}{t-s} (\log \|P_{s,t}f\|_1 + \log \frac{1}{2}) \\ &\leq \limsup_{t \rightarrow \infty} \frac{1}{t-s} (\log \mathbb{P}_m(\mathcal{E}) + \log \|f\|_\infty) \\ &= -E(\{A_r\}),\end{aligned}$$

completing the proof of $E(\{A_r\}) \leq -\Lambda_s(f)$.

A.7 Proof of Proposition 20

We start with proving the independence on the starting time.

Lemma 29: If $\lambda \in \sigma(\mathcal{P}_{s,s+\tau})$ for one $s \in \tau S^1$, then it holds for every $s \in \tau S^1$.

Proof. Let $s_1, s_2 \in \tau S^1$. Without loss $s_2 > s_1$, as elements of $[0, \tau)$. Since $\mathcal{P}_{s_1, s_1+\tau} = \mathcal{P}_{s_2, \tau+s_1} \mathcal{P}_{s_1, s_2}$, we have by the cyclical interchangeability of factors in the operator product without changing the spectrum of the product, that

$$\begin{aligned}\sigma(\mathcal{P}_{s_1, s_1+\tau}) &= \sigma(\mathcal{P}_{s_2, s_1+\tau} \mathcal{P}_{s_1, s_2}) \\ &= \sigma(\mathcal{P}_{s_1+\tau, s_2+\tau} \mathcal{P}_{s_2, s_1+\tau}) \\ &= \sigma(\mathcal{P}_{s_2, s_2+\tau}).\end{aligned}$$

□

Now we continue proving Proposition 20. For simplicity, let us write $\lambda_2 = \lambda_2(\mathcal{P}_{s,s+\tau})$. We show the first equality in (25) by showing first “ \geq ”, then “ \leq ”. One has (because the maximum is always taken with respect to functions satisfying $\int f = 0$)

$$\begin{aligned}\max_f \limsup_{t \rightarrow \infty} \frac{1}{t-s} \log \|P_{s,t}f\|_1 &\geq \max_f \limsup_{k \rightarrow \infty} \frac{1}{k\tau} \log \|\mathcal{P}_{s, s+k\tau}f\|_1 \\ &= \max_f \limsup_{k \rightarrow \infty} \frac{1}{k\tau} \log \left\| [\mathcal{P}_{s, s+\tau}]^k f \right\|_1 \\ &= \frac{1}{\tau} \log |\lambda_2|\end{aligned}\tag{49}$$

where the first inequality follows from restricting the lim sup to the times $\{k\tau\}_{k \in \mathbb{N}}$, and the next equation comes from the τ -periodicity of the vector field. The final equality can be obtained by noting that $\mathcal{P}_{s, s+\tau}$ is a compact operator (its spectrum has no accumulation points apart from 0), all eigenfunctions g at eigenvalues $\lambda \neq 1$ satisfy $g \perp \mathbb{1}$ (i.e. $\int g = 0$), and using the Riesz (spectral) decomposition at the eigenvalue λ_2 , which yields that the expression in the norm grows at most as $|\lambda_2|^k$.

To show the other inequality, let $[x]$ denote the integer part of $x \in \mathbb{R}$, and define $k(t) := \lfloor \frac{t-s}{\tau} \rfloor$. Then, by splitting the time interval $[s, t]$ into $[s, t - k(t)\tau]$ and $[t - k(t)\tau, t]$, we have

$$\|\mathcal{P}_{s,t}f\|_1 = \|\mathcal{P}_{t-k(t)\tau,t}\mathcal{P}_{s,t-k(t)\tau}f\|_1 \leq \|\mathcal{P}_{t-k(t)\tau,t}\|_{1,1^\perp} \|\mathcal{P}_{s,t-k(t)\tau}f\|_1, \quad (50)$$

where $\|\cdot\|_{1,1^\perp}$ denotes the induced L^1 operator norm on the (invariant) subspace $\{f \in L^1 \mid \int f = 0\}$. The invariance follows from $\int \mathcal{P}_{s,r}f = 0$ for every $r \geq s$ and $\int f = 0$. Thus, (50) yields

$$\begin{aligned} & \max_f \limsup_{t \rightarrow \infty} \frac{1}{t-s} \log \|\mathcal{P}_{s,t}f\|_1 \\ & \leq \max_f \limsup_{t \rightarrow \infty} \frac{1}{t-s} (\log \|\mathcal{P}_{t-k(t)\tau,t}\|_{1,1^\perp} + \log \|\mathcal{P}_{s,t-k(t)\tau}f\|_1) \\ & \leq \limsup_{t \rightarrow \infty} \frac{1}{t-s} \log \|\mathcal{P}_{t-k(t)\tau,t}\|_{1,1^\perp} + \max_f \limsup_{t \rightarrow \infty} \frac{1}{t-s} \log \|\mathcal{P}_{s,t-k(t)\tau}f\|_1 \end{aligned} \quad (51)$$

Now, due to periodicity of the forcing,

$$\mathcal{P}_{t-k(t)\tau,t} = [\mathcal{P}_{t-k(t)\tau,t-(k(t)-1)\tau}]^{k(t)},$$

and as in (49), we have that the first term in (51) is equal to $\frac{1}{\tau} \log |\lambda_2|$. For the second term, note that $t \mapsto \|\mathcal{P}_{s,t-k(t)\tau}f\|_1$ is a periodic function bounded from above by $\|f\|_1$ (this latter property being a consequence of the fact that $\mathcal{P}_{s,r}$ is a Markov operator). Consequently, $\limsup_{t \rightarrow \infty} \frac{1}{t-s} \log \|\mathcal{P}_{s,t-k(t)\tau}f\|_1 = 0$ for every f , and so is the right term in (51). This concludes the proof of Proposition 20.

A.8 Proof of Lemma 22 and Theorem 23

We start with a technical lemma collecting some properties of the transfer operator family. Extensive work has been done here [Kat61, DPG79, Paz83, AT85, AT87, Acq88, But92, Ama95, Lun95, PS01], unfortunately results on the L^1 -case in particular with explicit application to partial differential equations seem to be scarce. Here, we apply the results of [Tan96] and of [Ama83] to our specific setting.

Lemma 30: Let Assumption 12 hold, then the following are true.

(a) Let $t_* > s$ be arbitrary. The abstract (nonautonomous) evolution equation

$$\partial_t u_t = \mathcal{G}_t u_t, \quad u_s = f, \quad (52)$$

(i) has a unique solution $u \in C([s, t_*]; L^1) \cap C^1((s, t_*]; L^1)$, such that $u_t \in D(\mathcal{G}_t)$ for $s < t \leq t_*$. It is given by $u_t = \mathcal{P}_{s,t}f$ on L^1 ,

where the transfer operator family $\mathcal{P}_{s,t} : L^1 \rightarrow L^1$ satisfies

(ii) $\mathcal{P}_{s,r}\mathcal{P}_{r,t} = \mathcal{P}_{s,t}$ for all $s \leq r \leq t$;

(iii) there is a $C > 0$ such that $\|\partial_t \mathcal{P}_{s,t}\|_{L^1} = \|\mathcal{G}_t \mathcal{P}_{s,t}\|_{L^1} \leq \frac{C}{t-s}$ for all $s < t$.

(b) The operator $\mathcal{P}_{s,t} : L^1 \rightarrow L^1$ is compact for every $s < t$.

Proof. (a). The claims follow from [Tan96, Section 6.13], where the abstract evolution equation (52) in L^1 , corresponding to the partial differential equation (the Fokker–Planck equation (22)), is shown to satisfy the conditions (called assumptions (P1), (P2), and (P4) therein) that allow the application of the abstract results of Acquistapace and Terreni [AT86, AT87]. A solution satisfying (i) is called a *classical solution* therein [Tan96, Definition 6.1], its uniqueness and representation by the transfer operator family (called *fundamental solution* therein) are shown in [Tan96, Section 6.12, Theorem 6.6]. Property (ii) is a fundamental property of solutions (following from uniqueness), and (iii) is given in [Tan96, Section 6.10].

Next we have to show that under Assumption 12 the conditions of [Tan96] are satisfied for our Fokker–Planck equation (22). To this end, we need to define the boundary operator $B(t, x) \equiv B(x) : \xi \mapsto \langle n(x), \xi \rangle$ for $\xi \in \mathbb{R}^d$, where $n(x)$ is the unit outward normal at $x \in \partial X$. We define the Fokker–Planck differential operator $\mathcal{L}(t, x, \partial) := \frac{\varepsilon^2}{2} \sum_{i=1}^d \partial_i^2 - \sum_{i=1}^d (\partial_i v_i(t, x)) - \sum_{i=1}^d v_i(t, x) \partial_i$, as the right-hand side of the Fokker–Planck equation (22). Tanabe [Tan96, Section 6.13] requires that

- X is a bounded open domain of class C^4 (the order m of our differential operator \mathcal{L} is 2, and the domain has to be of class C^{2m}).
- The coefficients of the differential operator \mathcal{L} and boundary operator B should be Hölder continuous (of some positive order) in t . The same should hold for the coefficients of the adjoint boundary value problem (\mathcal{L}', B') .

It is immediate that Assumption 12 fulfills these conditions (note that the adjoint boundary conditions to the Neumann boundary conditions considered here, $B(\partial)u = 0$, are the very same conditions, i.e. $B' = B$). Further, it is required that the hypotheses of [Tan96, Section 5.3] are satisfied by the operators B, \mathcal{L} for every $t \in [s, t_*]$. These are the conditions of [Tan96, Theorems 5.5 and 5.6], i.e.

- local regularity of class C^{2m} and uniform regularity of class C^m of the domain X ;
- conditions (iii) and (iv) in [Tan96, Section 5.2];

and the conditions of [Tan96, Section 4.2]:

- smoothness conditions on the coefficients of the operator \mathcal{L} (boundedness and uniform continuity in x on \overline{X} is sufficient);
- uniform ellipticity of \mathcal{L} in X ;
- the so-called root condition for \mathcal{L} ;

- smoothness of the coefficients of the boundary operator (for us, it means differentiability with bounded and uniformly continuous derivatives, which is given, since the regularity class of the domain implies the smoothness of the outward normal $n(x)$ in x); and
- the so-called complementing condition for \mathcal{L} and B .

All of these are straightforward to check. The root condition is satisfied by strongly elliptic operators \mathcal{L} , cf. [Tan96, Theorem 5.4].

(b). By (iii) of part (a), we have that

$$\|\mathcal{G}_t \mathcal{P}_{s,t}\|_{L^1} \leq \frac{C}{t-s} \quad (53)$$

for $t > s$. Since \mathcal{G}_t is the L^1 -realization of the differential operator $\mathcal{L}(t, \cdot, \cdot)$, the inequality (53) imposes a certain smoothening property on $\mathcal{P}_{s,t}$. We will exploit this smoothness to show compactness of $\mathcal{P}_{s,t}$.

First note, that the regularity assumptions by Amann on the problem (the coefficients of the differential operator and the boundary parametrization), given in [Ama83, pp. 225 and pp. 235], are implied by our Assumption 12. It is shown in [Ama83, Proposition 9.2], that $D(\mathcal{G}_t)$ (imposed with the graph norm) is continuously embedded in the Sobolev space W_1^1 (weakly differentiable L^1 functions), i.e. there is a constant $\tilde{C} > 0$ such that for every $u \in D(\mathcal{G}_t)$ one has

$$\|u\|_{W_1^1} \leq \tilde{C} (\|\mathcal{G}_t u\|_{L^1} + \|u\|_{L^1}) . \quad (54)$$

Substituting (53) into (54), we have for $u = \mathcal{P}_{s,t} u_s$ that

$$\|\mathcal{P}_{s,t} u_s\|_{W_1^1} \leq \tilde{C} \left(\frac{C}{t-s} + 1 \right) \|u_s\|_{L^1} .$$

Thus, by the Rellich–Kondrachov theorem (which implies compact embedding of W_1^1 into L^1) we have that $\mathcal{P}_{s,t} : L^1 \rightarrow L^1$ is a compact operator for $s < t$.

We remark that the compactness of $\mathcal{P}_{s,t}$ on L^r , $1 < r < \infty$, is somewhat easier to obtain, since a bound as in (54) readily follows from the *Agmon–Douglis–Nirenberg estimate* [Tan96, (4.25) on pp. 131]. \square

Proof of Lemma 22. By the definition of \mathcal{G} we have

$$\partial_r \mathbf{f}(r, \cdot) = (\mathcal{G}_r - \mu) f_r , \quad r \in \tau S^1 . \quad (55)$$

Since $\mathcal{P}_{s,t}$ is the evolution operator of the parabolic evolution equation $\partial_r u(r) = \mathcal{G}_r u(r)$, we see that $e^{-\mu t} \mathcal{P}_{s,s+t} f_s$ solves (55). Uniqueness of the solutions to (55) in L^1 follows from Lemma 30, hence $f_{s+t \bmod \tau} = e^{-\mu t} \mathcal{P}_{s,s+t} f_s$. \square

Proof of Theorem 23. By Proposition 20 the left hand side of equation (27) is equal to $\frac{1}{\tau} \log |\lambda_2(\mathcal{P}_{s,s+\tau})|$. If \mathcal{G} has an eigenvalue μ then $\mathcal{P}_{s,s+\tau}$ has an eigenvalue $e^{\mu\tau}$, as shown

in Lemma 22. It remains to show, that $\mathcal{P}_{s,s+\tau}$ having an eigenvalue λ implies that \mathcal{G} has an eigenvalue μ such that $e^{\mu\tau} = \lambda$, with the corresponding eigenfunctions being equal too.

First note, that $\lambda \in \sigma(\mathcal{P}_{s,s+\tau})$ implies $\lambda \in \sigma(\mathcal{P}_{s+t,s+t+\tau})$ for every $t \geq 0$ by Lemma 29. Fix $s \in \tau S^1$, and let f_s be an eigenfunction of $\mathcal{P}_{s,s+\tau}$ with eigenvalue $\lambda \neq 0$. Further, let $\mu \in \mathbb{C}$ be any complex number such that $e^{\mu\tau} = \lambda$.

Define $f_{s+t} = e^{-\mu t} \mathcal{P}_{s,s+t} f_s$ for $t \geq 0$. It is easy to see that the consistency properties hold, i.e. $f_{s+\tau} = f_s$, and f_{s+t} is an eigenfunction of $\mathcal{P}_{s+t,s+t+\tau}$ at eigenvalue λ for any $t > 0$.

Lemma 30 (b) states that $f_{s+t} \in D(\mathcal{G}_{s+t})$ and differentiable with respect to t for every $t > 0$. Now, differentiate f_{s+t} with respect to t to obtain

$$\begin{aligned} \partial_t f_{s+t} &= -\mu e^{-\mu t} \mathcal{P}_{s,s+t} f_s + e^{-\mu t} \mathcal{G}_{s+t} \mathcal{P}_{s,s+t} f_s \\ &= -\mu f_{s+t} + \mathcal{G}_{s+t} f_{s+t} \end{aligned}$$

Rearranging terms yields that \mathbf{f} , defined by $\mathbf{f}(r, \cdot) = f_r$, is an eigenfunction of \mathcal{G} at the eigenvalue μ . The construction shows that $\operatorname{Re}(\mu) = \frac{1}{\tau} \log |\lambda|$. □

References

- [Acq88] Paolo Acquistapace. Evolution operators and strong solutions of abstract linear parabolic equations. *Differential and Integral Equations*, 1(4):433–457, 1988.
- [Ama83] Herbert Amann. Dual semigroups and second order linear elliptic boundary value problems. *Israel Journal of Mathematics*, 45.(2–3):225–254, 1983.
- [Ama95] Herbert Amann. *Linear and Quasilinear Parabolic Problems: Volume I: Abstract Linear Theory*, volume 1. Springer Science & Business Media, 1995.
- [Are02] H. Aref. The development of chaotic advection. *Physics of Fluids*, 14(4):1315–1325, 2002.
- [AT85] Paolo Acquistapace and Brunello Terreni. Maximal space regularity for abstract linear non-autonomous parabolic equations. *Journal of functional analysis*, 60(2):168–210, 1985.
- [AT86] Paolo Acquistapace and Brunello Terreni. On fundamental solutions for abstract parabolic equations. In *Differential equations in Banach spaces*, pages 1–11. Springer, 1986.
- [AT87] Paolo Acquistapace and Brunello Terreni. A unified approach to abstract linear nonautonomous parabolic equations. *Rendiconti del Seminario Matematico della Universita di Padova*, 78:47–107, 1987.

- [BR95] John Robert Baxter and Jeffrey S Rosenthal. Rates of convergence for everywhere-positive markov chains. *Statistics & probability letters*, 22(4):333–338, 1995.
- [But92] Anna Buttu. On the evolution operator for a class of non-autonomous abstract parabolic equations. *Journal of mathematical analysis and applications*, 170(1):115–137, 1992.
- [BVOB⁺10] Francisco J. Beron-Vera, María J. Olascoaga, Michael G. Brown, Huseyin Koçak, and Irina I. Rypina. Invariant-tori-like Lagrangian coherent structures in geophysical flows. *Chaos*, 20(2010):1–13, 2010.
- [CL99] Carmen Chicone and Yuri Latushkin. *Evolution semigroups in dynamical systems and differential equations*. Number 70. American Mathematical Soc., 1999.
- [DPG79] Giuseppe Da Prato and Pierre Grisvard. Equations d’évolution abstraites non linéaires de type parabolique. *Annali di Matematica Pura ed Applicata*, 120(1):329–396, 1979.
- [DY06] Mark F Demers and Lai-Sang Young. Escape rates and conditionally invariant measures. *Nonlinearity*, 19(2):377, 2006.
- [EN00] Klaus-Jochen Engel and Rainer Nagel. *One-parameter semigroups for linear evolution equations*, volume 194. Springer Science & Business Media, 2000.
- [FGTQ14] Gary Froyland, Cecilia Gonzalez-Tokman, and Anthony Quas. Detecting isolated spectrum of transfer and Koopman operators with Fourier analytic tools. *Journal of Computational Dynamics*, 1(2):249–278, 2014.
- [FJK13] Gary Froyland, Oliver Junge, and Péter Koltai. Estimating long-term behavior of flows without trajectory integration: The infinitesimal generator approach. *SIAM Journal on Numerical Analysis*, 51(1):223–247, 2013.
- [FLS10] Gary Froyland, Simon Lloyd, and Naratip Santitissadeekorn. Coherent sets for nonautonomous dynamical systems. *Physica D: Nonlinear Phenomena*, 239(16):1527 – 1541, 2010.
- [FP09] G. Froyland and K. Padberg. Almost-invariant sets and invariant manifolds – connecting probabilistic and geometric descriptions of coherent structures in flows. *Physica D*, 238:1507–1523, 2009.
- [FPG14] Gary Froyland and Kathrin Padberg-Gehle. Almost-invariant and finite-time coherent sets: directionality, duration, and diffusion. In *Ergodic Theory, Open Dynamics, and Coherent Structures*, pages 171–216. Springer, 2014.

- [FS10] Gary Froyland and Ognjen Stancevic. Escape rates and Perron–Frobenius operators: Open and closed dynamical systems. *Discrete and Continuous Dynamical Systems - Series B*, 14:457–472, 2010.
- [FS13] Gary Froyland and Ognjen Stancevic. Metastability, Lyapunov exponents, escape rates, and topological entropy in random dynamical systems. *Stochastics and Dynamics*, 13(04), 2013.
- [FSM10] Gary Froyland, Naratip Santitissadeekorn, and Adam Monahan. Transport in time-dependent dynamical systems: Finite-time coherent sets. *Chaos: An Interdisciplinary Journal of Nonlinear Science*, 20(4):043116, 2010.
- [HBV12] George Haller and Francisco J. Beron-Vera. Geodesic theory of transport barriers in two-dimensional flows. *Physica D: Nonlinear Phenomena*, 241(20):1680–1702, 2012.
- [HMS04] Wilhelm Huisinga, Sean Meyn, and Christof Schütte. Phase Transitions and Metastability in Markovian and Molecular Systems. *The Annals of Applied Probability*, 14(1):419–458, 2004.
- [How74] James S Howland. Stationary scattering theory for time-dependent hamiltonians. *Mathematische Annalen*, 207(4):315–335, 1974.
- [HP98] George Haller and A. C. Poje. Finite time transport in aperiodic flows. *Physica D: Nonlinear Phenomena*, 119(3):352–380, 1998.
- [JW02] Christopher Jones and Sean Winkler. Invariant manifolds and lagrangian dynamics in the ocean and atmosphere. *Handbook of dynamical systems*, 2:55–92, 2002.
- [Kar16] Daniel Karrasch. Lagrangian transport through surfaces in volume-preserving flows. *SIAM Journal on Applied Mathematics*, 76(3):1178–1190, 2016.
- [Kat61] Tosio Kato. Abstract evolution equations of parabolic type in Banach and Hilbert spaces. *Nagoya Mathematical Journal*, 19:93–125, 1961.
- [Kol10] Péter Koltai. *Efficient approximation methods for the global long-term behavior of dynamical systems – Theory, algorithms and examples*. PhD thesis, Technische Universität München, 2010.
- [KP92] Peter E Kloeden and Eckhard Platen. *Numerical Solution of Stochastic Differential Equations*. Springer, 1992.
- [LeV02] Randall J. LeVeque. *Finite Volume Methods for Hyperbolic Problems*. Cambridge University Press, 2002.

- [LM94] Andrzej Lasota and Michael C Mackey. *Chaos, fractals, and noise: stochastic aspects of dynamics*, volume 97. Springer, 1994.
- [Lun95] Alessandra Lunardi. *Analytic Semigroups and Optimal Regularity in Parabolic Problems*. Birkhäuser, 1995.
- [MMP84] RS MacKay, JD Meiss, and IC Percival. Transport in hamiltonian systems. *Physica D*, 13(1):55–81, 1984.
- [Øks03] Bernt Øksendal. *Stochastic differential equations*. Springer, 2003.
- [Paz83] Amnon Pazy. *Semigroups of linear operators and applications to partial differential equations*. Springer-Verlag, New York, 1983.
- [PS01] Jan Prüss and Roland Schnaubelt. Solvability and Maximal Regularity of Parabolic Evolution Equations with Coefficients Continuous in Time. *Journal of Mathematical Analysis and Applications*, 256(2):405–430, April 2001.
- [RBBV⁺07] I. I. Rypina, M. G. Brown, F. J. Beron-Vera, H. Koçak, M. J. Olascoaga, and I. A. Udovydchenkov. On the Lagrangian Dynamics of Atmospheric Zonal Jets and the Permeability of the Stratospheric Polar Vortex. *Journal of the Atmospheric Sciences*, 64(10):3595–3610, 2007.
- [RKLW90] V. Rom-Kedar, A. Leonard, and S. Wiggins. An analytical study of transport, mixing and chaos in an unsteady vortical flow. *Journal of Fluid Mechanics*, 214:347–394, 1990.
- [RKW90] V. Rom-Kedar and S. Wiggins. Transport in two-dimensional maps. *Archive for Rational Mechanics and Analysis*, 109:239–298, 1990.
- [RSR⁺00] Frank Rübiger, Roland Schnaubelt, Abdelaziz Rhandi, Jürgen Voigt, et al. Non-autonomous Miyadera perturbations. *Differential and Integral Equations*, 13(1-3):341–368, 2000.
- [Sch99] Roland Schnaubelt. Sufficient conditions for exponential stability and dichotomy of evolution equations. In *Forum Mathematicum*, volume 11, pages 543–566. Berlin; New York: De Gruyter, c1989-, 1999.
- [SHM03] Christof Schütte, Wilhelm Huisinga, and Sean Meyn. Metastability of diffusion processes. In *IUTAM Symposium on Nonlinear Stochastic Dynamics*, pages 71–81. Springer, 2003.
- [SLM05] Shawn C Shadden, Francois Lekien, and Jerrold E Marsden. Definition and properties of lagrangian coherent structures from finite-time lyapunov exponents in two-dimensional aperiodic flows. *Physica D: Nonlinear Phenomena*, 212(3):271–304, 2005.

- [SSA09] Mrityunjay K Singh, Michel FM Speetjens, and Patrick D Anderson. Eigenmode analysis of scalar transport in distributive mixing. *Physics of Fluids*, 21(9):093601, 2009.
- [Tan96] Hiroki Tanabe. *Functional analytic methods for partial differential equations*, volume 204. CRC Press, 1996.
- [Wig92] S. Wiggins. *Chaotic Transport in Dynamical Systems*. Springer-Verlag, New York, NY, 1992.
- [Wig05] Stephen Wiggins. The dynamical systems approach to lagrangian transport in oceanic flows. *Annu. Rev. Fluid Mech.*, 37:295–328, 2005.